

Fresh, Fair and Energy-Efficient Content Provision in a Private and Cache-Enabled UAV Network

Peng Yang, *Member, IEEE*, Kun Guo, *Member, IEEE*, Xing Xi, *Graduate Student Member, IEEE*, Tony Q. S. Quek, *Fellow, IEEE*, Xianbin Cao, *Senior Member, IEEE*, and Chenxi Liu, *Member, IEEE*

Abstract—In this paper, we investigate a private and cache-enabled unmanned aerial vehicle (UAV) network for content provision. Aiming at delivering fresh, fair, and energy-efficient content files to terrestrial users, we formulate a joint UAV caching, UAV trajectory, and UAV transmit power optimization problem. This problem is confirmed to be a sequential decision problem with mixed-integer non-convex constraints, which is intractable directly. To this end, we propose a novel algorithm based on the techniques of subproblem decomposition and convex approximation. Particularly, we first propose to decompose the sequential decision problem into multiple repeated optimization subproblems via a Lyapunov technique. Next, an iterative optimization scheme incorporating a successive convex approximation (SCA) technique is explored to tackle the challenging mixed-integer non-convex subproblems. Besides, we analyze the convergence of the proposed algorithm and derive the theoretical value of the expected peak age of information (PAoI) to estimate the content freshness. Simulation results demonstrate that the proposed algorithm can achieve the expected PAoI close to the theoretical value and is more 22.11% and 70.51% energy-efficient and fairer than benchmark algorithms.

Index Terms—Fresh content, private UAV network, UAV caching, trajectory design, power control

I. INTRODUCTION

THE data traffic requested by terrestrial mobile users will increase dramatically in terrestrial wireless mobile communication networks [2]. It is predicted that monthly data traffic in the global mobile networks will reach 77 exabytes by 2022 [2]. It is also foreseeable that with the advancement of manufacturing, chips, and sensors technologies, the global data traffic in future wireless networks will increase exponentially [3]. However, the flexibility and resilience of terrestrial network services are insufficient [4]. It is a challenging task for terrestrial networks to guarantee satisfactory network performance at any time, especially during peak traffic time [5].

Owing to the agile and resilient deployment, the unmanned aerial vehicle (UAV) network has been widely considered as a significant complement in 5G and beyond to terrestrial networks to boost the capacity of terrestrial networks and extend the network coverage [4]. Moreover, by deploying a private UAV network with complete control over some aspects (e.g., network resources and storage resources) of

the network, the private UAV network can provide further optimized services over the service area [6]. Recently, the research on the private UAV network attracts much attention from academia and industry [6]–[9].

On the other hand, UAV caching is a promising paradigm to assist terrestrial networks [10]. By proactively caching popular and repetitively requested content files with large size (e.g., high-resolution map, football match video), UAV caching can significantly alleviate the traffic burden and backhaul congestion of terrestrial networks in the peak hours of some hotspots [3], [5]. Besides, when content requests are hit by the caching, content files can be directly transmitted without traversing wireless backhaul, which reduces the response delay significantly [11]. On-demand UAV communications can also be dispatched when terrestrial networks are overloaded, the manner of which is flexible and cost-effective. As a result, during the past few years, the issue of UAV caching has been studied extensively [3], [5], [12]–[14].

A. Related work

In terms of the research on the private UAV network, the work in [6] deployed a private blockchain-enabled UAV 5G network to meet dynamic user demands in a reliable and secure manner. In [7], the UAV-aided interference assessment for private 5G new radio (NR) deployments was investigated. The utilization of dedicated portions of cellular spectrum to provide the high-reliable command and control link for UAVs was evaluated in [8]. Besides, the work in [9] designed optimal trajectories of UAVs in private UAV networks to always maintain connections between UAVs and a ground station under the constraint that the total distance travelled by all UAVs is minimum.

In terms of the research on the UAV caching, the work in [3] explored a cache-enabled UAV assisted wireless network to maximize the minimum throughput among UAV served users, by jointly optimizing the cache placement, UAV trajectory, and UAV transmit power in a finite flight period. In [5], the UAV-aided edge caching to assist terrestrial vehicular networks in delivering high-bandwidth content files was investigated. Besides, the issue of UAV caching for decreasing the transmission latency and alleviating backhaul congestion in a UAV network with limited wireless backhaul capacity was studied in [14]. Although the UAV caching issue was extensively discussed in [3], [5], [12]–[14] via optimizing cache placement and UAV trajectory, and so on, few of them discuss the problem of maintaining the “freshness” of cached contents. It is crucial

P. Yang, K. Guo, and T. Q. S. Quek are with the Information Systems Technology and Design, Singapore University of Technology and Design, 487372 Singapore. X. Xi, and X. Cao are with the School of Electronic and Information Engineering, Beihang University, Beijing 100083, China. C. Liu is with the State Key Laboratory of Networking and Switching Technology, Beijing University of Posts and Telecommunications, Beijing 100876, China. This paper was presented in part in the IEEE Global Communications Conference 2020 [1].

to deliver fresh content files to the destination nodes in some applications especially in some delay-sensitive applications, such as intelligent transportation, environmental monitoring, and health monitoring [15]. The outdated information may result in degraded user experience, erroneous control, even cause big catastrophes [16]. The “freshness” is an important metric, referred to as the age of information (AoI) or status age, which is defined as the amount of time elapsed since the instant at which the most recently delivered update takes place [17]. Due to the significance of delivering fresh content files, AoI-aware UAV-assisted wireless network design has attracted increasing interest from the research community [15], [16], [18]. For example, the work in [15] proposed to jointly optimize the UAV trajectory, the time required for energy harvesting, and data collection for each sensor node to minimize the average AoI of collected data in a UAV-assisted wireless network. The work in [18] investigated the problem of jointly optimizing the UAV trajectory, sensing time, transmission time, and task scheduling to guarantee the freshness of the UAV sensed data in a UAV network.

B. Motivation and contributions

Despite the extensive existing work on fresh data provision, all of them [15], [16], [18] focused on the issue of maintaining the freshness of data delivered to a single destination node from a single/multiple source nodes without discussing the significant problem of minimizing the AoI of data destined to multiple destination nodes. In fact, the investigation on the issue of delivering fresh data to multiple destination nodes is significant. On one hand, multiple UAVs instead of a single UAV should be deployed to deliver data to destination nodes owing to the limited service ability and coverage range of a single UAV. On the other hand, for delay-sensitive information (e.g., traffic information and live news), it is important to guarantee the freshness of delivered data.

The goal of minimizing the AoI of data delivered to multiple destination nodes, however, poses novel and greater challenges to the optimization of AoI and the theoretical analysis of AoI in a UAV-assisted wireless network. First, the minimization of AoI of data depends on the simultaneous decision making on data placement, data delivery, UAV trajectory, and UAV transmit power [15], [16], [18]. Multiple UAVs rather than a single UAV should be deployed to deliver fresh data to destination nodes. Nevertheless, the joint decision making on data placement, data delivery, UAV trajectory, and UAV transmit power in a multi-UAV network is much more challenging than that in a single UAV network studied in [15], [16], [18]. Besides, this joint decision making problem can be confirmed as a sequential decision problem with a high-dimensional and mixed discrete and continuous decision space. Therefore, it is difficult to explore some standard optimization methods and the popular deep reinforcement learning methods, which are designed either for the low-dimensional discrete decision space or the high-dimensional continuous decision space, to solve this problem. Although we considered multiple destination nodes for a joint decision making on UAV trajectory and UAV transmit power in our previous work [1], the issues of ensuring

fresh data delivery was not addressed. Second, owing to the complex interaction between multiple decision variables and the freshness of data, the theoretical analysis on the freshness of data destined to multiple destination nodes has not been well investigated.

To tackle the above challenges and provide further optimized services, we focus on the joint design of UAV caching (including content placement and content delivery), UAV trajectory, and UAV transmit power in a private and cache-enabled UAV network in this paper. The main contributions of this paper can be summarized as follows:

1) A time-varying UAV network is desired to be deployed to deliver fresh content to terrestrial users due to the limited UAV service ability and communication coverage range. In this regard, we formulate the problem of content provision by deploying a private and cache-enabled UAV network as a sequential decision problem. The goal of this problem is to maintain the freshness of data arriving at all users and provide fair and energy-efficient content delivery for all users, subject to UAVs’ transmit power and trajectory constraints.

2) To effectively solve the formulated problem, a Lyapunov-based optimization framework and a novel algorithm with provable performance guarantees are proposed. Particularly, the framework solves the complicated sequential decision problem via decomposing it into repeatedly optimized subproblems of multi-tier structure rather than solve it as a whole. The decomposed subproblems, however, are confirmed to be mixed-integer non-convex, which are still intractable directly. To make them tractable, the proposed algorithm firstly explores an iterative optimization scheme to handle the mixed-integer issue. Then, a successive convex approximation (SCA) technique is leveraged to tackle the non-convexity.

3) Besides, we analysis the convergence of the proposed algorithm. The theoretical value of the expected peak AoI (PAoI) to estimate the freshness of the content is also obtained by the probability theory.

4) Finally, the performance of the proposed algorithm is compared with different benchmark algorithms, and impact of different design parameters is discussed. Simulation results verify that the proposed algorithm can achieve the expected PAoI close to the theoretical value. Further, the proposed algorithm is more 22.11% and 70.51% energy-efficient and fairer than benchmark algorithms, respectively.

II. SYSTEM MODEL AND PROBLEM FORMULATION

A. Scenario description

This paper considers a content server and a private and cache-enabled UAV network, which includes one ground base station (BS), multiple UAVs, and many terrestrial mobile users, as shown in Fig. 1. The content server will proactively transmit content files, each of which consists of many data packets, requested by users to the BS such that the latency for users to obtain content files can be significantly reduced. However, terrestrial users, the set of which is $\mathcal{I} = \{1, 2, \dots, N\}$ with N being the number of users, may be in poor communication environment due to serious signal occlusion or too far from the BS. Then, the BS-user transmission links may be interrupted,

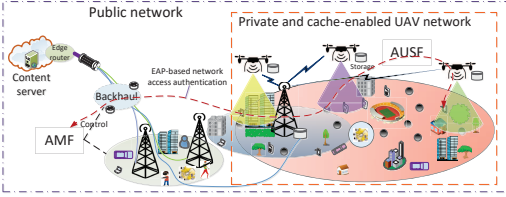


Fig. 1. The communication scenario and network architecture of a private and cache-enabled UAV network.

and users will have poor quality-of-experience (QoE). Hence, a set \mathcal{J} of J energy-constrained rotary-wing UAVs acting as aerial relays is deployed to perform the communication task of providing fresh, fair and energy-efficient content delivery for terrestrial users. In addition, to provide better direct content delivery services for terrestrial users, each UAV is equipped with a capacity-limited storage to dynamically cache content files from the BS and then deliver cached files to users.

To theoretically model the communication task, the time domain in the private and cache-enabled UAV network is assumed to be discretized. We consider a general case of assuming that the UAV communication task of delivering content files may last long enough, i.e., $t = \{1, 2, \dots\}$, and Δ_t is the duration of a time slot. Owing to the limited number of UAVs and a UAV's restricted communication range, the locations of UAVs should be continuously adjusted when executing the task such that UAVs can deliver content files to all terrestrial users.

B. Network architecture

In the above scenario, terrestrial users served by the UAVs need to access the content server residing in the public network. To this aim, we design a network architecture shown in Fig. 1. This network architecture includes a public network, a private and cache-enabled UAV network, and a BS shared by the public network and the private and cache-enabled UAV network (referred to as UAV network for brevity). For the BS, it is split into higher radio access layers (i.e., radio resource control (RRC), packet data control protocol (PDCP)) and lower-layer radio interface (i.e., radio link control (RLC), medium access control (MAC), physical layer (PHY)). The higher layers can be configured to operate in a user-specific mode. For example, for a user requiring low-latency services, RRC can be configured and tailored to disable the lower-layer Internet protocol (IP) stack and related header compression. Besides, RLC can be configured in transparent mode by the RRC. In contrast, for a user requiring high quality of experience (QoE), IP and acknowledged RLC should be initiated [19]. The UAV network and the public network will share the lower-layer radio interface of the BS. The higher radio access layers of the BS are split to the public network. Besides, the public network will provide core network functions.

To access the content server, a roaming agreement should be established between the public network and users in the UAV network [20]. This can be done by using a communication terminal or else just by using the subscriber identity in the public network. Yet, when sharing the BS, the network security

is one of the major concerns [20]. In 3GPP specified 5G networks, an extensible authentication protocol (EAP) based method (see [21]) can be introduced to ensure the security. In the considered scenario, the authentication is done between users and an authentication server function (AUSF) in the UAV network. This leads to keys shared between the AUSF and users. The keys are derived during authentication and are utilized to protect user traffic. According to [22], one of these keys is passed on towards the access and mobility management function (AMF) in the public network as a basis for establishing security between the mobile device and the public network. Another key agreed with the mobile during the same EAP run can however be retained by the private network and can be used to establish user plane security between users and the UAV network. Besides, network security is terminated by the PDCP. Making the split between the UAV network and the public network below the PDCP allows to keep all security related functions within the UAV network.

To instantiate the network architecture, the network function virtualization (NFV) and software-defined networking (SDN) techniques should be explored. NFV and SDN are complementary technologies that achieve the level of abstraction and flexibility required to satisfy stringent applications' requirements while maximizing network infrastructure reutilization [23]. Specifically, NFV can decouple physical network functions (PNFs) (e.g., firewalls, routers, load balancers) from dedicated hardware by implementing the same functionality in software, called virtualized network functions (VNFs) [23]. VNFs may then be instantiated in data centers at backend clouds, or on top of devices equipped with compute and storage resources at the edge [24]. For example, in the considered architecture, candidates for VNF instances include AUSF and AMF.

SDN can decouple the user plane from the control plane and centralize network management in an SDN controller. The network management can then be facilitated via a software-ization approach. With a global view of the network resources, SDN controller applications can take advantage of numerous southbound interfaces (e.g., OpenFlow, NETCONF) to gather network state information and act upon each forwarding device (PNF or VNF) accordingly. In the considered architecture, due to the exploration of the SDN technique, the control plane network functions (e.g., home subscribe server (HSS), AMF) can be deployed on the public network and shared by the UAV network. The public network and UAV network can maintain their own user plane network functions which are responsible for handling user-specific and bearer traffic.

Based on the above scenario and network architecture, we next mathematically model the communication task.

C. UAV caching model

As terrestrial users in general submit their content requests earlier than the expected time that content files are received, their content requests may be known in advance [25]. For any user $i \in \mathcal{I}$, denote by \Pr_i the probability of content requests of user i received by the content server with $\sum_{i=1}^N \Pr_i = 1$. According to the known content request information, decisions on UAV caching including the content placement and delivery, modelled as below, can then be made.

1) *Content placement model*: In the model, any terrestrial user may obtain its requested content files from one of the following two links, i.e., UAV cache-user link (if content files are cached in UAVs) and BS cache-UAV-user link¹. Denote by $\mathcal{F} = \{f_1, f_2, \dots, f_i, \dots, f_N\}$ a finite content library, where f_i represents the content file requested by user $i \in \mathcal{I}$. The size of each content file is assumed to be same² [5]. For any UAV $j \in \mathcal{J}$, denote by $b_{j,f_i}(t)$ a content placement decision variable at time slot t . $b_{j,f_i}(t) = 1$ if the content file f_i destined to user i is cached in UAV j . In this case, it is possible for user i to obtain the content file f_i from UAV j directly; otherwise, $b_{j,f_i}(t) = 0$. When $b_{j,f_i}(t) = 0$, user i has to obtain the content file f_i via the BS cache-UAV-user link. Just like [26], we assume that one user requests at most one content file and each UAV can cache at most one content file at time slot t . Then, we have the following content placement constraint

$$\sum_{f_i \in \mathcal{F}} b_{j,f_i}(t) \leq 1, \forall j, t. \quad (1)$$

2) *Content delivery model*: Denote by $s_{ij}(t)$, $\forall i, j, t$, the content delivery status of UAV j at time slot t . $s_{ij}(t) = 1$ represents that UAV j directly delivers the cached content file or forward the content file from the BS cache to user i at t . $s_{ij}(t) = 0$ indicates that UAV j does not deliver a content file to user i at t . Besides, each UAV can deliver a content file to one user, and one user can obtain the requested content file from one UAV at each time slot. Formally, we have

$$0 \leq \sum_j s_{ij}(t) \leq 1, \forall i, t, \quad 0 \leq \sum_i s_{ij}(t) \leq 1, \forall j, t \quad (2)$$

where we lighten $\sum_j s_{ij}(t)$ and $\sum_i s_{ij}(t)$ for $\sum_{j \in \mathcal{J}} s_{ij}(t)$ and $\sum_{i \in \mathcal{I}} s_{ij}(t)$, respectively. The similar lightened notation is adopted for brevity throughout the rest of this paper.

D. UAV power consumption and movement model

By referring to (2), we know that a terrestrial user cannot receive content files from a UAV at every time slot. Therefore, we investigate the time average communication behaviors of terrestrial users and UAVs in this paper.

1) *UAV power consumption model*: Given UAV j , define its time average transmit power during the first t time slots as $\bar{p}_j(t) = \frac{1}{t} \sum_{\tau=1}^t p_j(\tau)$ with $p_j(\tau)$ being the instantaneous transmit power of UAV j at time slot τ . Except for the transmit power, UAVs are subject to inherent circuit power consumption mainly including power consumption of mixers, frequency synthesizers, and digital-to-analog converters. Denote p_j^c as the circuit power of UAV j during a time slot, we then model the power consumption of UAV j at time slot t as

$$p_j^{tot}(t) = p_j(t) + p_j^c, \forall j, t, \quad (3)$$

which is upper-bounded by a constant \hat{p}_j , i.e., $p_j^{tot}(t) \leq \hat{p}_j$. Accordingly, the time average power consumption of UAV j during the first t time slots can be written as

$$\bar{p}_j^{tot}(t) = \bar{p}_j(t) + p_j^c, \forall j, t, \quad (4)$$

¹As the case of obtaining content files via the BS cache-user link was well studied in [3], [13], [14], [26], we did not investigate this type of link here.

²Note that different users may request the similar content file. For files with diverse sizes, the analysis can be extended by dividing each file into chunks of equal size.

which is constrained by $\bar{p}_j^{tot}(t) \leq \tilde{p}_j$, and \tilde{p}_j is a constant.

2) *UAV movement model*: At each time slot, all UAVs are movement controlled to execute the communication task efficiently. Denote the horizontal location of UAV $j \in \mathcal{J}$ as $\mathbf{x}_j(t) = [x_j(t), y_j(t)]^T$ at time slot t . Like [3], [5], we consider a scenario that all UAVs fly horizontally at a constant altitude g to achieve a lower level of energy consumption. During the flight, the distance between two consecutive waypoints on a UAV trajectory will be constrained by the UAV's maximum speed. As such, the mathematical expression of the waypoint distance constraint is given by

$$\|\mathbf{x}_j(t) - \mathbf{x}_j(t-1)\|^2 \leq e_{\max}^2, \forall j, t, \quad (5)$$

where e_{\max} is the UAV's maximum flight distance during a slot, $\mathbf{x}_j(0)$ represents the initial location of j .

Additionally, for collision avoidance, the distance between any two UAVs at each slot should not be less than a safety distance. Mathematically, the expression can be written as

$$\|\mathbf{x}_j(t) - \mathbf{x}_k(t)\|^2 \geq d_{\min}^2, \forall j, k \neq j, t, \quad (6)$$

where d_{\min} is the minimum safety distance.

E. Air-to-ground communications

For air-to-ground (AtG) communications, each terrestrial user may have a line-of-sight (LoS) view towards a UAV with a certain probability. A widely adopted expression of the LoS probability is [27]

$$\Pr(r_{ij}(t)) = [1 + a \exp(-b(\phi_{ij}(t) - a))]^{-1}, \forall i, j, t, \quad (7)$$

where a and b are constants relying on the type of environment, such as rural and dense urban, $\phi_{ij}(t) = \frac{180}{\pi} \times \arctan(\frac{g}{r_{ij}(t)})$ is the elevation angle of user i towards UAV j , $r_{ij}(t)$ denotes the horizontal distance between user $i \in \mathcal{I}$ and UAV $j \in \mathcal{J}$, i.e., $r_{ij}(t) = \|\mathbf{x}_j(t) - \mathbf{x}_i^u(t)\|$, and $\mathbf{x}_i^u(t) = [x_i^u(t), y_i^u(t)]^T$ represents the location of user i at time slot t , which can be known via a global positioning system (GPS).

Consider the setting that the user-altitude and antenna-heights of both user and UAV are neglected. The path-loss expression between user i and UAV j can be given by [27]

$$10 \log_{10}(h_{ij}(t)) = 20 \log_{10}(\frac{4\pi}{\varsigma}) + 20 \log_{10}(\sqrt{g^2 + r_{ij}^2(t)}) + \Pr(r_{ij}(t))\eta_{LoS} + (1 - \Pr(r_{ij}(t)))\eta_{NLoS}, \forall i, j, t, \quad (8)$$

where $\varsigma = c/f_c$ is the carrier wavelength, c (in m/s) is the speed of light, f_c (in Hz) is the carrier frequency, η_{LoS} (in dB) and η_{NLoS} (in dB) are losses corresponding to LoS and non line-of-sight (NLoS) connections.

In the considered UAV network, UAVs will hover during a time slot to deliver content files to terrestrial users. In this case, it is significant for UAVs to establish LoS links towards terrestrial users. This is because UAVs are energy-constrained and will consume much less power for content provision via LoS links than NLoS links [3], [12]. Therefore, we focus on the LoS AtG communications and then discuss the condition for establishing LoS connections between UAVs and users. According to statistical analysis results in [27], under the worst-case AtG propagation environment (i.e., dense urban),

the probability of a LoS AtG propagation link can be over 90%, when the elevation angle between a UAV and a user is not less than a threshold θ^{th} . Thus, we have the following condition for approximately establishing LoS AtG connections

$$\|\mathbf{x}_j(t) - \mathbf{x}_i^u(t)\| \leq g \tan^{-1} \theta^{\text{th}}, \forall i, j, t. \quad (9)$$

Under the approximated LoS AtG connection condition, we can approximate (8) as

$$h_{ij}(t) \approx G_{LoS} \zeta^2 / (16\pi^2 (D_{ij}(t))^2), \forall i, j, t, \quad (10)$$

where $G_{LoS} = 10^{-\eta_{LoS}/10}$, and $D_{ij}(t) = \sqrt{g^2 + r_{ij}^2(t)}$ is the distance between UAV j and user i at time slot t .

F. Quality-of-experience model

In this subsection, the concept of QoE is introduced to understand and improve the subjective perception of the quality of a network service as a whole by the end user [28]. We leverage a widely used mean opinion score (MOS) [28] to model the QoE of a user.

1) *Mean opinion score*: For any user i at time slot t , its MOS can take the following form [28]

$$\bar{D}_{i,f_i}(t) = \hat{D} - D_{i,f_i}(t) / (\hat{D} - L/u_{\text{dl}}^{\text{max}}), \forall i, t, \quad (11)$$

where \hat{D} is configured based on the desired system requirement [26], [28], $D_{i,f_i}(t)$ represents the edge transmission latency of user i , which is defined as the required time to transmit a content file from the BS or a UAV to user i at time slot t , $u_{\text{dl}}^{\text{max}} = \log_2 \left(1 + \frac{p_{\text{max}} G_{LoS} \zeta^2}{16\pi^2 g^2 \sigma^2 W} \right)$ (in bps/Hz), the constant $p_{\text{max}} = \hat{p}_j - p_j^c$, $\forall j$, is the maximum instantaneous transmit power of a UAV during each time slot, and $\sigma^2 W$ is the noise power with W (in MHz) being the total bandwidth.

User i will have a ‘‘very good’’ QoE state if $\bar{D}_{i,f_i}(t) \geq D^{\text{th}}$ [26], [28]. Here, D^{th} is the MOS threshold that maximizes the edge transmission latency of user i enjoying the desired ‘‘very good’’ QoE. (11) shows the interplay between the MOS and the edge transmission latency of user i at time slot t . We next model the edge transmission latency of user i , $\forall i \in \mathcal{I}$.

2) *Edge transmission latency model*: Recall that content files can be transmitted to terrestrial users via a BS cache-UAV-user link or a UAV cache-user link. Thus, during time slot t , the edge transmission latency for user i to receive a content file f_i can be given by

$$D_{i,f_i}(t) = \begin{cases} L/(Wu_i^{\text{dl}}(t)), & b_{j,f_i}(t) = 1 \\ D^{\text{ul}} + L/(Wu_i^{\text{dl}}(t)), & b_{j,f_i}(t) = 0 \end{cases} \quad (12)$$

where L (in Mbits) denotes the size of the transmitted content file, $u_i^{\text{dl}}(t)$ (in bps/Hz) is the achievable data rate of user i , and the constant D^{ul} represents the transmission latency of delivering the content file from the BS to a UAV³.

From (11), we know that improving users’ QoE indicates reducing the edge transmission latency of delivering content files. There is an inherent interplay between the edge transmission latency and data rate. We next model the data rate.

³The constant transmission latency can be achieved by exploring BS power control strategy, which has been investigated in our previous paper [29].

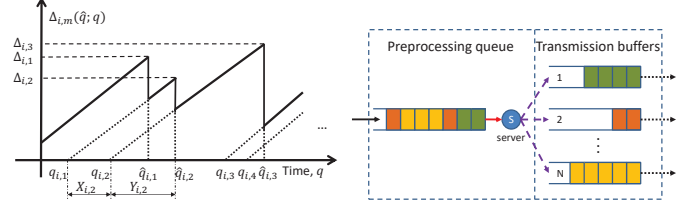


Fig. 2. An example of PAoI evolution Fig. 3. Management strategy of the model of packets towards user i [30]. BS for newly arrived packets.

3) *AtG data rate model*: By referring to (11) and (12), for any UAV j and user i , the required data rate (denoted by $C_{i,f_i}^{\text{th}}(t)$ (in bps/Hz)) for user i to achieve the desired QoE state when receiving the content file f_i can be written as

$$C_{i,f_i}^{\text{th}}(t) = \frac{L \sum_{j \in \mathcal{J}_i} b_{j,f_i}(t)}{W(\hat{D} - D^{\text{th}}(\hat{D} - L/(Wu_{\text{dl}}^{\text{max}})))} + \frac{L(1 - \sum_{j \in \mathcal{J}_i} b_{j,f_i}(t))}{W(\hat{D} - D^{\text{th}}(\hat{D} - L/(Wu_{\text{dl}}^{\text{max}})) - D^{\text{ul}})}, \forall i, t, \quad (13)$$

where $\mathcal{J}_i(t)$ denotes a set of UAVs with horizontal distances towards user i being small than e_{max} at time slot t .

Next, we use Shannon capacity to quantify the receiving data rate (in bps/Hz) of user i from UAVs at time slot t , i.e.,

$$u_i^{\text{dl}}(t) = \sum_j s_{ij}(t) \log_2 \left(1 + \frac{p_j(t) h_{ij}(t)}{\sigma^2 W + I_{ij}(t)} \right), \forall i, t, \quad (14)$$

where $I_{ij}(t) = \sum_{k \in \mathcal{J} \setminus \{j\}} p_k(t) h_{ik}(t)$ denotes the interference experienced at user i when all UAVs share the spectrum. Then, the condition of $u_i^{\text{dl}}(t) \geq C_{i,f_i}^{\text{th}}(t)$ should be satisfied if user i 's achievable data rate can enable its desired QoE state.

G. PAoI evolution model of packets

Different from AoI, PAoI provides information of the maximum value of AoI and can capture the extent to which update information is stale [30]. Therefore, just like [30], we adopt the PAoI as the metric to estimate the freshness of information. Additionally, we discuss the above models from the perspective of content files, each of which includes a batch of packets. However, as most PAoI-related work [30], [31] discuss the PAoI evolution from the viewpoint of data packets, we next model the PAoI evolution of packets.

For any user $i \in \mathcal{I}$, define the AoI of a packet m destined to user i as $\Gamma_{i,m}(q) = q - q_{i,m-1}$, where $q_{i,m-1}$ is the generation time of the most recently received packet $m-1$ from the data server until time q [17].⁴ When user i does not receive packet m , the value of $\Gamma_{i,m}(q)$ increases linearly with q , which in turn shows the fact that packet m is getting older. In other words, the m -th peak value of $\Gamma_{i,m}(q)$ is obtained right before the m -th newly generated packet arrives at user i . The m -th peak value of $\Gamma_{i,m}(q)$ is defined as the PAoI [30], denoted by $\Delta_{i,m}(\hat{q}; q)$, where \hat{q} denotes the time that a packet generated at time q arrives at its destination user. Fig. 2 shows an example of the PAoI evolution model $\Delta_{i,m}(\hat{q}; q)$ for user i and packet

⁴The timescale of modelling of PAoI differs from that in the above models. This is because the inter-arrival time of packets is different from that of transmitting content files to users. For clarification, we use the terminology ‘time’ and the corresponding notation ‘ q ’ when analyzing PAoI of packets.

m .⁵ Formally, for any user i and packet m , the PAoI of packet m destined to user i evolves as follows [30]

$$\Delta_{i,m}(\hat{q}; q) = \begin{cases} \hat{q}_{i,m} & m = 1 \\ X_{i,m} + Y_{i,m} & m > 1 \end{cases} \quad (15)$$

where $\hat{q}_{i,m}$ is the time that packet m reaches user i , $X_{i,m} = q_{i,m} - q_{i,m-1}$, $Y_{i,m} = \hat{q}_{i,m} - q_{i,m}$, and $q_{i,m}$ is the generation time of packet m towards user i , as shown in Fig. 2.

The inter-arrival time $X_{i,m}$ is related to the packet arrival rate of packets sent to user i . The value of $Y_{i,m}$ is determined by many factors, such as the time cost of preprocessing data packets in the BS and the edge arrival duration. Specifically, for the BS, it will maintain a queue with infinite buffer space to manage arrived data packets, as shown in Fig. 3. Upon arriving at the BS, data packets will enter into the BS queue to wait to be preprocessed (e.g., packet classification, packet header update) according to a first-come-first-served (FCFS) principle. We call this queue the preprocessing queue. After being preprocessed, packets destined to different users will be cached at diverse transmission buffers maintained by the BS or forwarded and cached in UAVs. Therefore, we can re-write $Y_{i,m}$ as $Y_{i,m} = Y_{i,m}^Q + Y_{i,m}^S + Y_{i,m}^A$, where $Y_{i,m}^Q$ denotes the queuing delay of packet m , $Y_{i,m}^S$ is the preprocessing time of packet m in the content file f_i , and $Y_{i,m}^A \leq D_{i,f_i}(t)$ is the edge arrival duration of packet m . It is noteworthy that the values of $X_{i,m}$, $Y_{i,m}^Q$, and $Y_{i,m}^S$ are determined by some network parameters such as backhaul capacity and CPU computing speed and cannot be reduced by optimizing the deployment and resource (e.g., UAV transmit power) allocation of the UAV network [30]; yet, $Y_{i,m}^A$ can be optimized. In the following subsection we formulate an optimization problem of reducing the value of $Y_{i,m}^A$ while providing fair and energy-efficient content file delivery for all terrestrial users via the joint design of UAV caching, UAV trajectory, and UAV transmit power.

H. Problem formulation

Improving users' achievable data rates will result in reduced edge arrival duration and the following fresher content file transmission. Thus, a goal of the problem is to maximize users' achievable data rates. During the first t time slots, the time average achievable data rate of user i , $\forall i$, is written as $\bar{u}_i^{\text{dl}}(t) = \frac{1}{t} \sum_{\tau=1}^t u_i^{\text{dl}}(\tau)$. Define $\phi(\{\bar{u}_i^{\text{dl}}(t)\}) = \sum_i \log_2(1 + \bar{u}_i^{\text{dl}}(t))$ as a proportional fairness function of time average achievable data rates across all terrestrial users. Then, maximizing $\phi(\{\bar{u}_i^{\text{dl}}(t)\})$ will result in fresh and fair content provision for all users. Besides, to implement the energy-efficient content file delivery, the power consumption of UAVs should be minimized. To achieve the above goals, the joint optimization of UAV caching, UAV trajectory, and UAV transmit power should be investigated. Mathematically, we can formulate the joint optimization problem as below

$$\begin{aligned} & \text{Maximize}_{\mathcal{B}(t), \mathcal{S}(t), \mathcal{P}(t), \mathcal{X}(t)} \quad \liminf_{t \rightarrow \infty} (\phi(\{\bar{u}_i^{\text{dl}}(t)\}) - \rho \sum_j \bar{p}_j^{\text{tot}}(t)) \\ & \text{s.t.} \quad \liminf_{t \rightarrow \infty} [\bar{u}_i^{\text{dl}}(t) - \bar{C}_{i,f_i}^{\text{th}}(t)] \geq 0, \forall i \end{aligned} \quad (16a)$$

$$\text{s.t.} \quad \liminf_{t \rightarrow \infty} [\bar{u}_i^{\text{dl}}(t) - \bar{C}_{i,f_i}^{\text{th}}(t)] \geq 0, \forall i \quad (16b)$$

⁵Like [30], [31], we discuss the PAoI evolution of packets in the discrete time domain.

$$\limsup_{t \rightarrow \infty} \bar{p}_j^{\text{tot}}(t) \leq \tilde{p}_j, \forall j \quad (16c)$$

$$p_j^{\text{tot}}(t) \leq \hat{p}_j, \forall j, t \quad (16d)$$

$$s_{ij}(t) \in \{0, 1\}, \forall i, j, t \quad (16e)$$

$$b_{j,f_i}(t) \in \{0, 1\}, \forall j, t \quad (16f)$$

$$p_j(t) \geq p_j^{\text{min}}, \forall j, t \quad (16g)$$

$$(1), (2), (5), (6), (9). \quad (16h)$$

where $\mathcal{B}(t)$, $\mathcal{S}(t)$, $\mathcal{P}(t)$, and $\mathcal{X}(t)$ represent the sets of content placement decision variables, content delivery decision variables, UAV transmit power, and UAV locations at time slot t , respectively, ρ is a non-negative coefficient that weighs the trade-off between fresh and fair content delivery and power consumption, p_j^{min} is a small constant, $\bar{C}_{i,f_i}^{\text{th}}(t) = \frac{1}{t} \sum_{\tau=1}^t \varphi C_{i,f_i}^{\text{th}}(\tau)$ with $\varphi = \frac{J}{N}$. The constant φ is introduced because the condition $u_i^{\text{dl}}(t) \geq C_{i,f_i}^{\text{th}}(t)$ should be satisfied if user i 's "very good" QoE state can be achieved at time slot t . However, user i cannot receive a content file from a UAV at each time slot. Besides, each user has the probability of $\frac{J}{N}$ to receive the content file from a UAV due to the goal of achieving fair content delivery.

The solution to (16) is quite challenging mainly because i) *time-coupled objective function*: the objective function is the logarithmic function of time average achievable data rates. The calculation of the objective function requires the obtaining of all users' achievable data rates over the first t time slots, which indicates the optimization of a great number of decision variables. Besides, the number of decision variables in the problem will exponentially increase with an increasing t , which seriously hinders the solution to the problem; ii) *sequential decision problem*: it needs to optimize the UAV cache placement scheme, UAV cache delivery strategy, UAV transmit power, and UAV trajectories during the first t time slots; iii) *thorny optimization problem*: (16) includes a logarithmic-quadratic objective function, non-convex constraints (explained in detail in Section III), and continuous and integer variables. Therefore, (16) is a mixed-integer non-convex optimization problem that may be NP-hard or even undecidable.

To solve this highly challenging problem, we propose a Lyapunov-based optimization framework. In this framework, we first attempt to decouple the objective function of (16) in terms of time slots. Next, we leverage a Lyapunov drift-plus-penalty technique [32] to further decompose the problem with a time-decoupled objective function into multiple repeatedly optimized subproblems. Finally, an iterative optimization scheme is designed to tackle the mixed-integer non-convex characteristic of the subproblems.

III. LYAPUNOV-BASED OPTIMIZATION FRAMEWORK

Observing that the objective function is the logarithmic function of time average achievable data rates, we refer to the objective function as time-coupled objective function. We first leverage the Jensen inequality to decouple the time-coupled objective function. A sequential decision problem with a time-decoupled objective function can then be obtained, which is still difficult to be solved effectively. Reinforcement learning

(RL) approaches, such as Q-learning [33], and deep deterministic policy gradient (DDPG) [34], can be explored to solve sequential decision problems. However, Q-learning-based approaches can only handle discrete and low-dimensional action spaces, and DDPG-based methods are designed for continuous (real valued) action spaces [34]. (16) simultaneously involves discrete and continuous action spaces, which indicates that it will be highly difficult to design RL approaches to solve (16). What's more, RL approaches suffer from lack of complete theoretical basis.

To solve the sequential decision problem effectively, we propose a Lyapunov-based optimization framework, which decomposes the problem into multiple repeatedly optimized subproblems rather than solve this problem as a whole. The procedure of the framework is as follows.

A. Decouple of the objective function

Let $\gamma(t) = (\gamma_1(t), \dots, \gamma_N(t))$ be an auxiliary vector with $0 \leq \gamma_i(t) \leq u_{\text{dl}}^{\text{max}}, \forall i, t$. Define $g(t) = \phi(\gamma(t)) = \sum_i \log_2(1 + \gamma_i(t))$. Then, according to the Jensen's inequality, we can achieve $\bar{g}(t) \leq \phi(\bar{\gamma}(t))$. With this important inequality, the following Proposition shows that we can equivalently transform the original problem into a new one with a time-decoupled objective function.

Proposition 1. The original problem (16) can be equivalently transformed into the following sequential decision problem.

$$\underset{\mathcal{B}(t), \mathcal{S}(t), \mathcal{P}(t), \mathcal{X}(t), \gamma(t)}{\text{Maximize}} \quad \liminf_{t \rightarrow \infty} (\bar{g}(t) - \rho \sum_j \bar{p}_j^{\text{tot}}(t)) \quad (17a)$$

$$\text{s.t.} \quad \liminf_{t \rightarrow \infty} [\bar{u}_i^{\text{dl}}(t) - \bar{\gamma}_i(t)] = 0, \forall i \quad (17b)$$

$$\liminf_{t \rightarrow \infty} [\bar{u}_i^{\text{dl}}(t) - \bar{C}_{i, f_i}^{\text{th}}(t)] \geq 0, \forall i \quad (17c)$$

$$\liminf_{t \rightarrow \infty} [\bar{p}_j - \bar{p}_j^{\text{tot}}(t)] \geq 0, \forall j \quad (17d)$$

$$0 \leq \gamma_i(t) \leq u_i^{\text{max}}, \forall i, t \quad (17e)$$

$$(16d) - (16h). \quad (17f)$$

Proof. Please refer to Appendix A. \square

B. Lyapunov drift-plus-penalty

In this subsection, we leverage a Lyapunov drift-plus-penalty technique [32] to tackle the time average constraints in (17). Specifically, to enforce the constraint (17c), we introduce a family of virtual queues $\{Q_i(t)\}$ as the following

$$Q_i(t) = Q_i(t-1) + \varphi C_{i, f_i}^{\text{th}}(t) - u_i^{\text{dl}}(t-1), \forall i, t. \quad (18)$$

It can be concluded that the constraint (17c) is satisfied if the following mean-rate stability condition holds [32]

$$\lim_{t \rightarrow \infty} \mathbb{E}\{[Q_i(t)]^+\}/t = 0, \forall i, \quad (19)$$

where the non-negative operation $[x]^+ = \max\{x, 0\}$.

Likewise, to enforce the time average constraints (17b) and (17d), we define the virtual queues $Z_i(t)$, and $H_j(t)$, respectively, as

$$Z_i(t) = Z_i(t-1) + \gamma_i(t-1) - u_i^{\text{dl}}(t-1), \forall i, t, \quad (20)$$

$$H_j(t) = H_j(t-1) + p_j^{\text{tot}}(t-1) - \bar{p}_j, \forall j, t. \quad (21)$$

(17b) and (17d) can be satisfied, if the following mean-rate stability conditions can be held

$$\lim_{t \rightarrow \infty} \mathbb{E}\{[Z_i(t)]^+\}/t = 0, \forall i, \quad (22)$$

$$\lim_{t \rightarrow \infty} \mathbb{E}\{[H_j(t)]^+\}/t = 0, \forall j. \quad (23)$$

With the definitions of the virtual queues $[Q_i(t)]^+$, $[Z_i(t)]^+$, and $[H_j(t)]^+$, we can define a Lyapunov function $L(t)$ as a sum of square of these virtual queues at time slot t , i.e., $L(t) \triangleq \frac{1}{2} \sum_i ([Q_i(t)]^+)^2 + \frac{1}{2} \sum_i ([Z_i(t)]^+)^2 + \frac{1}{2} \sum_j ([H_j(t)]^+)^2$. $L(t)$ is a scalar measure of constraint violations. Intuitively, if the value of $L(t)$ is small, the absolute values of all queues are small; otherwise, the absolute value of at least one queue is great. Additionally, we define a drift-plus-penalty function as $\Delta(t) - V \left(g(t) - \rho \sum_j p_j^{\text{tot}}(t) \right)$, where $\Delta(t) = L(t+1) - L(t)$ represents a *Lyapunov drift*, $- \left(g(t) - \rho \sum_j p_j^{\text{tot}}(t) \right)$ is a *penalty*, and V is a non-negative penalty coefficient that weighs the trade-off between constraint violations and optimality. Lemma 1 presents the upper bound of the function value.

Lemma 1. At each time slot t , the upper bound of the value of the drift-plus-penalty function $\Delta(t) - V \left(g(t) - \rho \sum_j p_j^{\text{tot}}(t) \right)$ can be expressed as (24) with $B \triangleq \sum_i (u_{\text{dl}}^{\text{max}})^2 + \sum_j (\bar{p}_j)^2 / 2$

$$\begin{aligned} \Delta(t) - V \left(g(t) - \rho \sum_j p_j^{\text{tot}}(t) \right) \leq & B - \\ & \sum_j [H_j(t)]^+ (\bar{p}_j - p_j^c) + V \rho \sum_j p_j^c + \\ & \sum_i [Q_i(t)]^+ \varphi C_{i, f_i}^{\text{th}}(t) - V \phi(\gamma(t)) + \\ & \sum_i [Z_i(t)]^+ \gamma_i(t) + \sum_j \{V \rho + [H_j(t)]^+\} p_j(t) - \\ & \sum_i \{[Q_i(t)]^+ + [Z_i(t)]^+\} u_i^{\text{dl}}(t). \end{aligned} \quad (24)$$

Proof. Please refer to Appendix B. \square

In (24), the right-hand-side expression constitutes the upper bound of the drift-plus-penalty. As such, the minimization of the drift-plus-penalty can be approximated by minimizing its upper bound. We therefore mitigate (16) by greedily minimizing the upper bound of the drift-plus-penalty function at each t . Meanwhile, at each t , the upper bound can be decomposed into four independent terms including a constant term, an auxiliary variable term, a term related to content caching, and a term consisting of content delivery strategies, UAV transmit power as well as UAV trajectories. As a result, the Lyapunov-based optimization framework of mitigating (16) can be summarized as the following repeated optimization subproblems of three-tier structure.

- At each time slot t , observe $Q_i(t)$, $Z_i(t)$, $H_j(t)$ for any user $i \in \mathcal{I}$, and UAV $j \in \mathcal{J}$.
- *AUXiliary-Tier (AUT) optimization:* Choose $\gamma_i(t)$ for each user i to mitigate (25)

$$\underset{\gamma(t)}{\text{Minimize}} \quad -V \phi(\gamma(t)) + \sum_i [Z_i(t)]^+ \gamma_i(t) \quad (25a)$$

$$\text{s.t.} \quad 0 \leq \gamma_i(t) \leq u_{\text{dl}}^{\text{max}} \quad (25b)$$

- *Content-Placement-Tier (CPT) optimization*: Determine the content placement decision variable $b_{j,f_i}(t)$ for each UAV j to optimize (26)

$$\text{Minimize}_{\mathcal{B}(t)} \sum_i [Q_i(t)]^+ C_{i,f_i}^{\text{th}}(t) \quad (26a)$$

$$\text{s.t.} \quad \text{constraint (1)}. \quad (26b)$$

- *Delivery-Power-and-Trajectory-Tier (DPT²) optimization*: Given UAV trajectories $\mathcal{X}(t-1)$, choose $\mathcal{S}(t)$, $\mathcal{P}(t)$, and $\mathcal{X}(t)$ to mitigate (27)

$$\text{Minimize}_{\mathcal{S}(t), \mathcal{P}(t), \mathcal{X}(t)} \sum_j \{V\rho + [H_j(t)]^+\} p_j(t) - \sum_i \{[Q_i(t)]^+ + [Z_i(t)]^+\} u_i^{\text{dl}}(t) \quad (27a)$$

$$\text{s.t.} \quad (2), (5), (6), (9), (16d) - (16g). \quad (27b)$$

- Compute $u_i^{\text{dl}}(t)$ using (14). Update there virtual queues using (18), (20), and (21).

As shown in the above framework, the solution of (16) lies in the optimization of some subproblems. In this section, we present the detailed procedure of solving it.

C. AUT optimization

As the proportional fairness function $\phi(\gamma(t))$ is a separable sum of individual logarithmic functions, the mitigation of (25) is equivalent to a separate selection of the individual auxiliary variable $\gamma_i(t) \in [0, u_{\text{dl}}^{\text{max}}]$ for each user $i \in \mathcal{I}$ that minimizes a convex function $-V \log_2(1 + \gamma_i(t)) + [Z_i(t)]^+ \gamma_i(t)$ with respect to (w.r.t.) $\gamma_i(t)$. Thus, the closed-form solution to (25) can be written as

$$\gamma_i(t) = \begin{cases} u_{\text{dl}}^{\text{max}}, & [Z_i(t)]^+ = 0 \\ \min \left\{ \left[\frac{V}{[Z_i(t)]^+ \ln 2} - 1 \right]^+, u_{\text{dl}}^{\text{max}} \right\}, & \text{else} \end{cases} \quad (28)$$

D. CPT optimization

The goal of (26) is to reduce the data rate requirements of all terrestrial users. To this aim, content files should be cached in UAVs. As a result, the total power of all UAVs can be reduced when delivering content files to terrestrial users. Minimizing the total power of all UAVs is equal to the maximization of the reduction of transmit power of each UAV brought by content caching [26]. Thus, we can design the following content placement scheme to solve (26)

$$b_{j,f_i}(t) = \begin{cases} 1, & i = i^* \\ 0, & \text{otherwise} \end{cases} \quad (29)$$

where

$$i^* = \arg \max_{i \in \mathcal{N}_j} [Q_i(t)]^+ (p_j(\beta) - p_j(\alpha)), \quad (30)$$

and \mathcal{N}_j is the set of terrestrial users with the horizontal distance towards UAV j at time slot t being small than e_{max} , $p_j(\beta) - p_j(\alpha)$ represents the transmit power reduction of UAV j due to the content caching. Besides, UAV j will cache the content for its nearest user if $\mathcal{N}_j = \emptyset$. $\beta = \frac{L}{(\hat{D} - D^{\text{th}})(\hat{D} - L/u_{\text{dl}}^{\text{max}}) - D^{\text{ul}}}$, $\alpha = \frac{L}{(\hat{D} - D^{\text{th}})(\hat{D} - L/u_{\text{dl}}^{\text{max}})}$, and $p_j(\varpi) = \frac{(2^{\varpi/W} - 1)(\sigma^2 W + I_{ij}(t))}{h_{ij}(t)}$.

Remark 2: From (29) and (30), we can see that the content placement decision will be made based on the states (e.g., UAV locations) of the UAV network at the current time slot. Besides, the content placement depends on the pre-knowledge of content request of each terrestrial user and users' locations, which corresponds to the result given in [26].

E. DPT² optimization

It can be observed that (27) includes logarithmic-quadratic terms and continuous and integer variables. Besides, the constraint (16f) is non-convex; thus, (27) is a mixed-integer non-convex programming problem that is difficult to be addressed directly.

To address this challenge, we first propose to tackle the mixed-integer issue of (27) by leveraging an iterative optimization scheme. Particularly, the solution to (27) includes the iterative optimization of content delivery decision variables, UAV trajectory, and transmit power. Second, we explore an SCA technique [35] to approximately convert the generated non-convex optimization problems during the iterative optimization into convex ones.

1) *Content delivery decision variable optimization*: For given UAV trajectories $\mathcal{X}(t)$ and transmit power $\mathcal{P}(t)$, the content delivery strategy of (27) can be developed by solving the following problem

$$\text{Maximize}_{\mathcal{S}(t)} \sum_i \sum_j c_{ij}(t) s_{ij}(t) \quad (31a)$$

$$\text{s.t.} \quad (2), (16e). \quad (31b)$$

where $c_{ij}(t) = \{[Q_i(t)]^+ + [Z_i(t)]^+\} \log_2 \left(1 + \frac{p_j(t) h_{ij}(t)}{\sigma^2 W + I_{ij}(t)} \right)$.

It is easy to know that (31) is an integer linear programming problem and can be efficiently solved by some optimization tools such as MOSEK.

2) *UAV trajectory optimization*: Given the UAV transmit power $\mathcal{P}(t)$, UAV trajectories at time slot $t-1$, $\mathcal{X}(t-1)$, and the content delivery decision variable set $\mathcal{S}(t)$, (27) is still difficult to be solved by some standard optimization methods due to the non-convex objective function and constraint (6). To solve this problem effectively, an SCA technique [35] is exploited to tackle the non-convexity and approximately transform the non-convex optimization problem into a convex one. The key idea of SCA is to solve a sequence of convex optimization problems with different initial points to obtain an approximate solution to a non-convex optimization problem instead of solving the hard non-convex problem directly. The following Proposition presents the approximately transformed convex UAV trajectory optimization problem.

Proposition 2. By exploring the SCA technique, UAV trajectories at time slot t can be obtained by mitigating the following convex optimization problem.

$$\text{Maximize}_{\mathcal{X}(t), \{\eta_i(t)\}, \{B_{ik}(t)\}} \sum_i \{[Q_i(t)]^+ + [Z_i(t)]^+\} \eta_i(t) \quad (32a)$$

$$\text{s.t.} \quad \sum_j s_{ij}(t) (D_i^{(r)}(t) - \sum_{k \in \mathcal{J}} E_{ik}^{(r)}(t) (\|\mathbf{x}_k(t) - \mathbf{x}_i^{\text{u}}(t)\|^2 - \|\mathbf{x}_k^{(r)}(t) - \mathbf{x}_i^{\text{u}}(t)\|^2)) + \sum_j s_{ij}(t) \tilde{R}_{ij}(t) \geq \eta_i(t), \forall i, t \quad (32b)$$

$$B_{ik}(t) \leq \|\mathbf{x}_k^{(r)}(t) - \mathbf{x}_i^u(t)\|^2 +$$

$$2(\mathbf{x}_k^{(r)}(t) - \mathbf{x}_i^u(t))^T (\mathbf{x}_k(t) - \mathbf{x}_i^u(t)), \forall i, k \neq j, t \quad (32c)$$

$$- \|\mathbf{x}_j^{(r)}(t) - \mathbf{x}_k^{(r)}(t)\|^2 + 2(\mathbf{x}_j^{(r)}(t) - \mathbf{x}_k^{(r)}(t))^T \times$$

$$(\mathbf{x}_j(t) - \mathbf{x}_k(t)) \geq d_{\min}^2, \forall j, k \neq j, t \quad (32d)$$

$$(5), (9) \quad (32e)$$

where $\eta_i(t)$ and $B_{ik}(t)$ are slack variables,
 $D_i^{(r)}(t) = \log_2(\sigma^2 W + \sum_{k \in \mathcal{J}} \frac{p_k(t)\theta_{ij}}{g^2 + \|\mathbf{x}_k^{(r)}(t) - \mathbf{x}_i^u(t)\|^2}),$
 $E_{ik}^{(r)}(t) = \frac{p_k(t)\theta_{ij}}{(g^2 + \|\mathbf{x}_k^{(r)}(t) - \mathbf{x}_i^u(t)\|^2)^2 2^{D_i^{(r)}(t)} \ln 2}, \tilde{R}_{ij}(t) =$
 $-\log_2(\sigma^2 W + \sum_{k \in \mathcal{J} \setminus \{j\}} \frac{p_k(t)\theta_{ij}}{g^2 + B_{ik}(t)}), \theta_{ij} = \frac{G_{L, \text{QoS}} S^2}{16\pi^2}, \mathbf{x}_j^{(r)}(t),$
 and $\mathbf{x}_k^{(r)}(t)$ are given locations of UAV j and UAV k at the r -th iteration of the SCA technique.

Proof. Please refer to Appendix C. \square

Remark 3: The objective function (32a) is linear. As the left-hand-side (LHS) of (32b) is concave w.r.t. both $\mathbf{x}_k(t)$ and $B_{i,k}(t)$, it is a convex constraint. (32c) and (32d) are linear constraints. Besides, both (9) and (5) are convex quadratic constraints. Thus, (32) is now convex and can be efficiently mitigated by MOSEK. It is noteworthy that the lower-bounded approximation conducted in (32b)-(32d) shows that the feasible domain of (32) is smaller than that of (27). Hence, the opposite optimal value of (32a) is the upper bound of that of (27).

3) *UAV transmit power optimization:* Given the content delivery decision variable set $\mathcal{S}(t)$ and UAV trajectories $\mathcal{X}(t)$, it is still hard to mitigate (27) owing to the non-convex objective function. Likewise, the SCA technique is explored to tackle the non-convexity. The following Proposition shows a method of optimizing UAV transmit power.

Proposition 3. By exploring an SCA technique, the UAV transmit power at time slot t can be configured by mitigating the following convex optimization problem.

$$\begin{aligned} & \underset{\mathcal{P}(t), \{\eta_i(t)\}}{\text{Maximize}} && -V\rho \sum_j p_j(t) - \sum_j [H_j(t)]^+ p_j(t) + \\ & && \sum_i \{[Q_i(t)]^+ + [Z_i(t)]^+\} \eta_i(t) \end{aligned} \quad (33a)$$

$$\text{s.t. } \sum_j \left(s_{ij}(t) \hat{R}_{ij}(t) - s_{ij}(t) F_{ij}^{(r)}(t) \right) - \sum_j (s_{ij}(t) \times$$

$$\sum_{k \in \mathcal{J} \setminus \{j\}} G_{ik}^{(r)}(t) (p_k(t) - p_k^{(r)}(t))) \geq \eta_i(t), \forall i, t \quad (33b)$$

$$\eta_i(t) \geq s_{ij}(t) C_{i,f_i}^{\text{th}}(t), \forall i, j, t \quad (33c)$$

$$(16d), (16g) \quad (33d)$$

where $\hat{R}_{ij}(t) = \log_2(\sigma^2 W + \sum_{k \in \mathcal{J}} \frac{p_k(t)\theta_{ij}}{g^2 + \|\mathbf{x}_k(t) - \mathbf{x}_i^u(t)\|^2}),$
 $F_{ij}^{(r)}(t) = \log_2(\sigma^2 W + \sum_{k \in \mathcal{J} \setminus \{j\}} p_k^{(r)}(t) h_{ik}(t)), G_{ik}^{(r)}(t) =$
 $\frac{h_{ik}(t)}{2^{F_{ij}^{(r)}(t)} \ln 2},$ and $p_k^{(r)}(t)$ is the given transmit power of UAV k at the r -th iteration of SCA technique. (33c) is enforced due to the data rate requirement of enabling a user's desired QoE state.

Proof. Please refer to Appendix D. \square

Remark 4: The objective function (33a) is linear. As the LHS of (33b) is concave w.r.t. $p_k(t)$, it is a convex constraint.

Then, we can conclude that (33) is convex that can be efficiently alleviated by MOSEK. Similarly, the utilization of the approximation results in that the feasible set of (33) is a subset of that of (27). Therefore, the optimal opposite value of (33a) is the upper bound of that of (27).

Based on the above derivation, the main steps of the iterative optimization scheme of solving (27) can be summarized in Algorithm 1.

Algorithm 1 Iterative UAV content delivery, trajectory, and transmit power optimization

- 1: **Initialization:** Randomly initialize $\mathcal{X}^{(0)}(t)$ and $\mathcal{P}^{(0)}(t)$, let $r = 0$.
 - 2: **repeat**
 - 3: Given $\mathcal{X}^{(r)}(t), \mathcal{P}^{(r)}(t)$, solve (31) to obtain the optimal solution $\mathcal{S}^{(r+1)}(t)$.
 - 4: Given $\mathcal{S}^{(r+1)}(t), \mathcal{X}^{(r)}(t), \mathcal{P}^{(r)}(t)$, solve (32) to generate the optimal solution $\mathcal{X}^{(r+1)}(t)$.
 - 5: Given $\mathcal{S}^{(r+1)}(t), \mathcal{X}^{(r+1)}(t), \mathcal{P}^{(r)}(t)$, solve (33) to obtain the optimal solution $\mathcal{P}^{(r+1)}(t)$.
 - 6: Update $r = r + 1$.
 - 7: **until** Convergence or $r = r_{\max}$.
-

Finally, we can summarize the main steps of Lyapunov-based optimization framework of solving the original problem (16) in Algorithm 2.

Algorithm 2 Fresh, Fair, and Energy-Efficient Content Provision (F²E²CP)

- 1: **Initialization:** Initialize $Q_i(1) \in [0, 1], Z_i(1) \in [0, 1], H_j(1) \in [0, 1]$ for all user $i \in \mathcal{I}$, UAV $j \in \mathcal{J}$.
 - 2: **for** each time slot $t = 1, 2, \dots, T$ **do**
 - 3: Observe the virtual queues $Q_i(t), Z_i(t)$, and $H_j(t)$.
 - 4: Compute $\gamma_i(t)$ using (28) for all user i .
 - 5: Compute $b_{j,f_i}(t)$ using (29) for all UAV j .
 - 6: Obtain the content delivery decision set $\mathcal{S}(t)$, UAV trajectories $\mathcal{X}(t)$, and UAV transmit power $\mathcal{P}(t)$ using Algorithm 1.
 - 7: Calculate $p_j^{\text{tot}}(t)$ for all UAV j using (3).
 - 8: Calculate $u_i^{\text{dl}}(t)$ for all user i using (14).
 - 9: Update $Q_i(t+1), Z_i(t+1)$, and $H_j(t+1)$ for all user i and UAV j using (18), (20), and (21), respectively.
 - 10: **end for**
-

IV. PERFORMANCE ANALYSIS

In this section, the convergence performance of the proposed algorithms is analyzed. Observing that the PAoI of a data packet varies with many time-varying factors (e.g., inter-arrival time of the packet and packet queueing delay), the analysis on the PAoI of a data packet in the average sense is conducted.

A. Convergence analysis

The following Lemma shows that the convergence and validity of Algorithms 1 and 2 can be guaranteed.

Lemma 2. Algorithm 1 is convergent, and Algorithm 2 can make all virtual queues mean-rate stable.

Proof. Please refer to Appendix E. \square

B. Analysis of expected PAoI

Recall that many factors such as the inter-arrival time of a packet, packet queueing delay in the preprocessing queue, packet preprocessing time, and the edge arrival duration will contribute to the PAoI of a packet. We next analyze these factors in detail.

1) *Packet queueing delay analysis:* The analysis on the packet queueing delay requires the study of packet queueing behavior. To study the packet queueing behavior, the queue evolution process that involves the arrival, accumulation and departure of packets should be investigated.

During time q , once received the content requests of users during time q , the content server will generate and send out packets required by the users. To facilitate the analysis, a Poisson distribution with intensity (or the average number of new packets) $\vartheta_w(q)$ is explored to model the random and independent packet arrivals in the BS. As mentioned in the system model, once arrival, new packets will not be processed immediately and will enter the preprocessing queue to wait to be preprocessed. If the packet preprocessing rate, which is determined by the CPU computing speed [30], is slower than the packet arrival rate, some packets will be accumulated in the preprocessing queue. After being preprocessed, packets will depart from the preprocessing queue. In this regard, the packet departure rate is equal to the packet preprocessing rate. Denote by $N_a(q)$ the accumulated number of packets in the preprocessing queue at time q . The value of $N_a(q)$ is simultaneously determined by the following three factors: a) the accumulated number of packets; b) the number of new arrivals during $q - 1$, which will be counted at at time q ; c) the packet departure rate; thus, we can present the evolution model of $N_a(q)$ as follows

$$N_a^q = \begin{cases} 0, & q = 1 \\ [N_w^{q-1} - n_c]^+, & q = 2 \\ [N_w^{q-1} + N_w^{q-1} - n_c]^+, & q \geq 3 \end{cases} \quad (34)$$

where we write x^q instead of $x(q)$ to lighten the notation. N_w^{q-1} is the number of new arrivals in time $q-1$, the subtraction operation of n_c is performed because $n_c = \frac{r}{\kappa l}$ packets can be preprocessed during each time interval, l is the packet size (in bits), r is the CPU computing speed of the preprocessor with the units CPU cycles per second, and κ is a scaling parameter depending on the specific operation conducted on the packet with the units being CPU cycles per bit [30]. As new arrivals in the 1-st time interval will be counted in the 2-nd time interval and there are no accumulated packets in the 1-st time interval, we have $N_a^1 = 0$.

Based on the above evolution model, we have the following Lemma that derives the closed-form expressions of the accumulated number of packets in the preprocessed queue and the packet queueing delay of a newly arrival packet at time q .

Lemma 3. The accumulated number of packets in the queue can be approximated as Poisson distribution. As such, the

average number of accumulated packets in the queue at time $q > 1$ can be derived as

$$\vartheta_a^q = \left[\vartheta_w^{q-1} + \vartheta_a^{q-1} - n_c(1 - e^{-\vartheta_w^{q-1} - \vartheta_a^{q-1}}) \right]^+. \quad (35)$$

Besides, the average packet queueing delay of a newly arrival packet m sent to user i at time $q > 1$ is $\vartheta_a^q Y_{i,m}^S$.

Proof. Please refer to Appendix F. \square

2) *Analysis of the expected edge arrival duration:* We know that a content file including a batch of packets will be delivered from the BS or a UAV to a destination user in each time slot t . Then, we attempt to tackle the following issue: *What is the expected edge arrival duration for transmitting a packet?* The following Proposition gives the answer.

Proposition 4. For any user i and packet m , the expected edge arrival duration of packet m destined to user i can be given by

$$\mathbb{E}[Y_{i,m}^A] = \frac{(l+L)N\Delta t}{2JL} \quad (36)$$

where $\mathbb{E}[\cdot]$ represents an expectation operation.

Proof. Please refer to Appendix G. \square

3) *Closed-form expression of expected PAoI:* Based on the obtained results in Lemma 3 and Proposition 4, we can derive the closed-form expression of the expected PAoI of a packet in the following Lemma.

Lemma 4. The expected PAoI of packet m , which is generated at time q and sent to user i , $\forall i$, can be expressed as

$$\mathbb{E}[\Delta_{i,m}(\hat{q}; q)] = \begin{cases} \frac{1}{n_c} + \frac{(l+L)N\Delta t}{2JL} & q = 1, m = 1 \\ \frac{1}{\lambda_i^q} + \frac{1}{n_c} + \frac{\vartheta_a^q}{n_c} + \frac{(l+L)N\Delta t}{2JL} & q > 1, m > 1 \end{cases} \quad (37)$$

where $\lambda_i^q = \vartheta_w^q \text{Pr}_i$ is the intensity of new arrival packets destined to user i at time q .

Proof. Please refer to Appendix H. \square

V. SIMULATION RESULTS

A. Comparison algorithms and parameter setting

To verify the effectiveness of the proposed Algorithm 2, we compare it with five benchmark algorithms: 1) *Static UAV caching with power control (SUWPC) algorithm:* It randomly generates horizontal locations for N hovering UAVs with the same deployment altitude g . The proposed UAV transmit power optimization method is adopted in the algorithm. Besides, each UAV randomly delivers a cached or forwarded content file to terrestrial users within its LoS coverage region at each time slot after receiving users' content requests; 2) *Static UAV caching without power control (SUPC) algorithm:* The unique difference between SUPC and SUWPC lies in that SUPC adopts the maximum UAV transmit power to deliver content files to terrestrial users; 3) *Circular trajectory-based joint optimization (CTJO) algorithm:* Each UAV flies in a circular trajectory with a speed of 10 m/s. At the beginning of the simulation, UAVs are deployed in line with an equal interval. The distance between two adjacent UAVs is $1/4J$

km. The horizontal locations of the first and the last UAVs are $(1/4 + 1/\lfloor 8J \rfloor, 1/4)$ km and $(1/2 - 1/\lfloor 8J \rfloor, 1/4)$ km, respectively, and turning radiuses of them are $1/\lfloor 8N \rfloor$ km and $1/4 - 1/\lfloor 8J \rfloor$ km. In CTJO, all UAVs are deployed at the same altitude g . Besides, the proposed UAV caching and UAV transmit power optimization methods are utilized in this algorithm. 4) *Circular trajectory-based UAV caching (CTUC) algorithm*: The unique difference between CTUC and CTJO is that CTUC adopts the maximum UAV transmit power to deliver content files to terrestrial users. 5) *Circular trajectory without UAV caching (CTWUC) algorithm*: The unique difference between CTWUC and CTJO is that UAVs do not cache content files and will randomly forward content files from the BS to users in CTWUC.

We consider an urban area of size 0.5×0.5 km² with high-rise buildings, where terrestrial users are randomly distributed and moving. This scenario corresponds to the AtG channel environment of the worst case [27]. The radio frequency propagation parameters are: $\eta_{LoS} = 2.3$, carrier frequency $f_c = 4.9$ GHz, speed of light $c = 3.0 \times 10^8$ m/s, $\theta^{\text{th}} = 70^\circ$, $\sigma^2 = -174$ dBm/Hz, total bandwidth $W = 100$ MHz, $\hat{D} = 24$ s, $D^{\text{ul}} = 5$ s, $L = 150$ Mbits, $D^{\text{th}} = 0.6$, $\Delta_t = \hat{D} - D^{\text{th}}(\hat{D} - L/(Wu_{\text{dl}}^{\text{max}}))$ s [26], [27]. The default values of parameters related to UAVs and terrestrial users are: $\tilde{p}_j = 450$ mW, $\hat{p}_j = 500$ mW, $p_j^c = 20$ mW, $p_j^{\text{min}} = 1$ mW, $\forall j$, $p_{\text{max}} = 480$ mW, $e_{\text{max}} = 250$ m, $g = 200$ m, $d_{\text{min}} = 50$ m, $J = 4$, and $N = 50$. Expected PAoI analysis related parameters are: $l = 5000$ Bytes, $\gamma/\kappa = 1$ Mbits/s, $\vartheta_w^q \sim \text{Pois}(\frac{\gamma}{T})$, and $\text{Pr}_i = 1/N$, $\forall i, q$ [30]. Other system parameters are listed as follow: $r_{\text{max}} = 200$, $V = 0.01$, $T = 500$, and $\rho = 0.1$ [1].

B. Performance evaluation

In this subsection, we conduct simulations to comprehensively understand the availability of the developed F²E²CP algorithm. Besides, we repeat all comparison algorithms for fifteen times to eliminate the influence of some randomly initialized parameters such as UAV transmit power and locations on the performance evaluation. The final simulation result is the average of the obtained fifteen results.

First, we design a simulation to verify the effectiveness of the F²E²CP algorithm under the default parameter setting. Particularly, we plot the tendency of the virtual queue stability values, defined as $S_Q = \max_i [Q_i(t)]^+/t$, $S_Z = \max_i [Z_i(t)]^+/t$, and $S_H = \max_j [H_j(t)]^+/t$ in Fig. 4. Besides, the two-dimensional (2D) trajectories of four UAVs in the first 150 time slots and their final 2D positions are plotted in Fig. 5.

The following observations can be achieved from these figures: 1) the obtained queue stability values are bounded during the whole content provision period; 2) the obtained queue stability values tend to zero with an increasing time slot; as a result, all introduced virtual queues are mean-rate stable according to (19), i.e., all time average constraints in (17) can be imposed. This result verifies the effectiveness of the proposed F²E²CP algorithm; 3) the movement constraints of each UAV can be satisfied at each time slot.

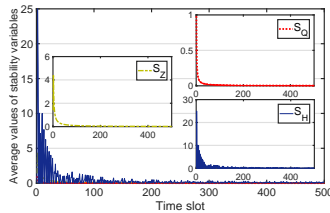


Fig. 4. Trend of virtual queue stability values vs. time slot.

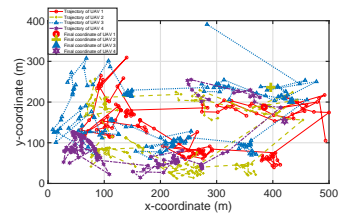
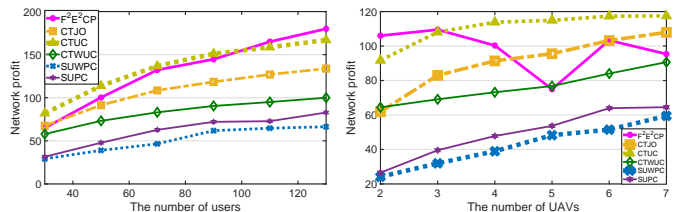
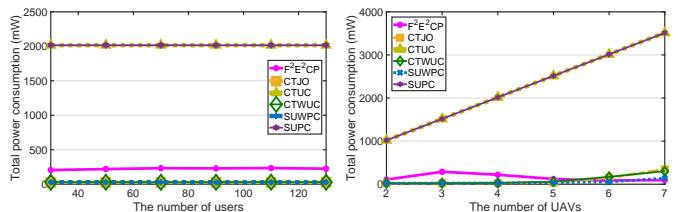


Fig. 5. Trajectories of four UAVs projected in a 2D space.



(a) Network profit vs. the number of users (b) Network profit vs. the number of UAVs

Fig. 6. Comparison of the obtained network profit.



(a) Total UAV power consumption vs. (b) Total UAV power consumption vs. N J

Fig. 7. Comparison of the obtained total UAV power consumption of all comparison algorithms.

Next, we conduct a simulation to testify the performance of F²E²CP by comparing it with other five benchmark algorithms. To quantify the algorithm performance, the following key performance indicators are introduced: the network profit that is defined as $\phi(\{\bar{u}_i^{\text{dl}}(T)\})$, the total UAV transmit power consumption that is calculated by $\sum_j \tilde{p}_j^{\text{tot}}(T)$, the energy efficiency that is computed by (16a), the Jain's fairness index, defined as $(\sum_i \bar{u}_i^{\text{dl}})^2 / N \sum_i (\bar{u}_i^{\text{dl}})^2$ with $\bar{u}_i^{\text{dl}} = \frac{1}{T} \sum_{t=1}^T u_i^{\text{dl}}(t)$, the expected PAoI of a packet computed by (37), where the obtained $\mathbb{E}[Y_{i,m}^A] = N(l+L)T\Delta_t / (2L \sum_{t=1}^T \sum_i \sum_j s_{ij}(t))$.

In Figs. 6 and 7, the influence of the number of users and UAVs on the obtained network profit and the total UAV power consumption is plotted. The tendency of the obtained energy efficiency and Jain's fairness indexes of all comparison algorithms are depicted in Figs. 8 and 9, respectively. Besides, in Fig. 8, the energy efficiency results of two comparison algorithms (i.e., CTUC and SUPC) are not plotted. This is because they suggest to transmit content files with the maximum UAV transmit power, and will achieve smaller energy efficiency values than other UAV power control-based algorithms. In Fig. 9, the fairness index results of CTJO and SUWPC are not plotted. As CTJO and SUWPC achieve smaller network profit than CTUC and SUPC, CTJO and SUWPC will obtain smaller Jain's fairness indexes.

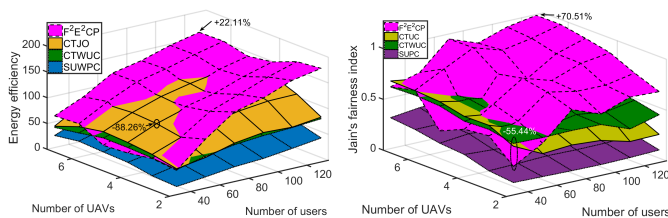


Fig. 8. Energy efficiency vs. N and Fig. 9. Jain's fairness index vs. N and J .

From these figures, we can observe that: 1) for all algorithms, their achieved network profit increases with an increasing number of users because content files can be successfully delivered to more users; 2) CTUC obtains the greatest network profit when $N \leq 90$, followed by the proposed F²E²CP algorithm. This is mainly because CTUC adopts the maximum UAV transmit power that results in great AtG data rates. Although SUPC adopts the scheme of transmitting content files with the maximum UAV transmit power, small network profit is obtained as many terrestrial users are experiencing outage throughout the content provision period. The observations show that the design of suitable UAV trajectories can help improve network profit; 3) except for F²E²CP, the obtained network profit of other comparison algorithms increase with an increasing number of UAVs. For F²E²CP, a great number of UAVs does not lead to big network profit. This is due to the complex impact of signal interference. For other comparison algorithms, the distance between any two UAVs is large. As a result, they can increase UAV transmit power to achieve greater network profit. Yet, the nearest distance between two UAVs can be 50 m which may result in large signal interference. To reduce signal interference, F²E²CP decreases the UAV transmit power when $J \geq 4$; 4) the generated total power consumption of all algorithms almost does not vary with the number of users because a UAV can deliver a content file to one user at each time slot. When $J < 5$, F²E²CP consumes greater UAV transmit power than other three comparison algorithms adopting the proposed UAV transmit power optimization method such that greater network profit can be gained; 5) when $N \leq 90$ and $J \leq 5$, CTJO may be energy-efficient than F²E²CP. For example, when $N = 50$ and $J = 4$, the obtained energy efficiency of the proposed F²E²CP algorithm is 88.26% of CTJO. However, from Fig. 6, we can find that F²E²CP may obtain higher network profit than CTJO under the similar parameter setting. This observation shows that F²E²CP tends to deliver content files to fewer users continuously when users are sparsely distributed, resulting from a small N . When the number of users and UAVs becomes great, F²E²CP can achieve greater energy efficiency than the CTJO algorithm. For instance, when $N = 130$ and $J = 7$, F²E²CP is energy-efficient by 22.11% than CTJO. The above result indicates that a simple circular UAV trajectory is preferable when terrestrial users are sparsely distributed in the considered communication area. However, when users are densely distributed, optimizing UAV trajectory will greatly improve the energy efficiency of content provision. Besides, CTJO may be energy-efficient than

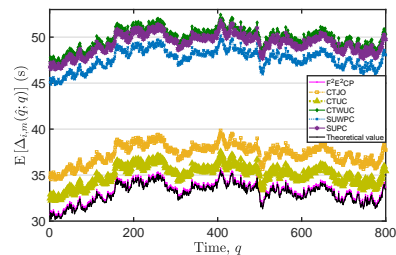


Fig. 10. Comparison of expected PAOI of all comparison algorithms.

CTWUC, which means that the UAV caching can improve the energy efficiency of content provision. SUWPC provides inefficient content delivery due to the static UAV deployment; 6) similarly, when the number of users is small (i.e., $N \leq 50$), F²E²CP may be overwhelmed by CTUC and CTWUC in terms of fair content provision. For example, when $N = 30$ and $J = 2$, the obtained fairness index of F²E²CP is 58.62% and 55.44% of that of CTUC and CTWUC, respectively. However, when $N > 50$, F²E²CP can provide fairer content delivery services for terrestrial users than CTUC, CTWUC, and SUPC. For instance, the obtained Jain's fairness index of F²E²CP is 1.70, 1.88, and 3.04 times of CTWUC, CTUC, and SUPC, respectively, when $N = 130$ and $J = 7$.

We plot the tendency of expected PAOI obtained by all comparison algorithms in Fig. 10 to show whether the expected PAOI can be reduced by the joint design of UAV caching, UAV trajectory, and UAV transmit power. In Fig. 10, the expected PAOI is obtained with $N = 30$ and $J = 5$.

From this figure, we can observe: 1) the proposed F²E²CP algorithm achieves a small value of expected PAOI that is close to the theoretical value. The obtained values of $\mathbb{E}[\Delta_{i,m}(\hat{q}; q)]$ of other comparison algorithms are much greater than the theoretical value. Besides, the two circular UAV trajectory-based algorithms with UAV caching achieve smaller $\mathbb{E}[\Delta_{i,m}(\hat{q}; q)]$ than the two static UAV trajectory-based algorithms. This observation shows the importance of UAV trajectory optimization in delivering fresh packets to terrestrial users; 2) CTWUC obtains the largest $\mathbb{E}[\Delta_{i,m}(\hat{q}; q)]$ and takes at least 12.57 seconds more than CTJO and CTUC to deliver packets to users. It indicates that UAV caching can significantly reduce the latency of delivering packets to users; 3) it is interesting to find that the UAV power control method alone cannot effectively reduce the expected edge arrival duration. For example, CTUC achieves smaller $\mathbb{E}[\Delta_{i,m}(\hat{q}; q)]$ than CTJO, yet, SUPC obtains greater $\mathbb{E}[\Delta_{i,m}(\hat{q}; q)]$ than SUWPC.

Summarily, the above simulation results indicate that the joint design of UAV caching, UAV trajectory, and UAV transmit power can guarantee the provision of fresh, fair, and energy-efficient content files for terrestrial users.

VI. CONCLUSION AND FUTURE WORK

This paper investigated a private and cache-enabled UAV network for providing fresh, fair, and energy-efficient content delivery services for terrestrial users. To achieve this goal, we formulated a joint UAV caching, UAV trajectory, and UAV transmit power optimization problem. We proposed a

novel algorithm by leveraging a Lyapunov-based optimization framework integrating an iterative optimization scheme and an SCA technique to solve the formulated problem. Besides, we discussed the convergence behaviour of the proposed algorithm as well as derived the theoretical value of expected PAoI of data packets. Simulation results verified that the proposed algorithm could provide fresh content files for users and was more 22.11% and 70.51% energy-efficient and fairer than benchmark algorithms. This paper explored an optimization method to design UAV trajectories in a 2D space. How to incorporate reinforcement learning with optimization to solve the joint UAV caching, three-dimensional UAV trajectory, and UAV transmit power optimization problem is a topic worthy of research in the near future.

APPENDIX

A. Proof of Proposition 1

Suppose all limits in (17) exist, the constraint (17b) is therefore equivalent to $\bar{u}_i^{\text{dl}}(t) = \bar{\gamma}_i(t)$. $\bar{g}(t) \leq \phi(\bar{u}_1^{\text{dl}}(t), \dots, \bar{u}_N^{\text{dl}}(t))$ can then be achieved. It means that the maximum value of the objective function of (17) is no greater than that of (16). Besides, the maximum value of the objective function of (16) can be obtained through letting $\bar{\gamma}_i(t) = \bar{u}_i^{\text{dl};*}(t)$ for all $i \in \mathcal{I}$, and $t \in \{1, 2, \dots\}$ with $(\bar{u}_1^{\text{dl};*}(t), \dots, \bar{u}_N^{\text{dl};*}(t))$ being the optimal time average achievable data rates of all users for (16) [32]. It indicates that the feasible domain of (16) is smaller than that of (17). Therefore, (17) and (16) are equivalent. This completes the proof.

B. Proof of Lemma 1

We discuss the upper bound of $\frac{1}{2}([Q_i(t+1)]^+)^2$ in three cases. According to (18) and the non-negative operation,

Case I: when $Q_i(t+1) \geq 0$ and $Q_i(t) \geq 0$, we can obtain

$$\begin{aligned} \frac{1}{2}([Q_i(t+1)]^+)^2 &= \frac{1}{2}([Q_i(t)]^+)^2 + \\ &[Q_i(t)]^+(\varphi C_{i,f_i}^{\text{th}}(t) - u_i^{\text{dl}}(t)) + \\ &\frac{1}{2}(\varphi C_{i,f_i}^{\text{th}}(t) - u_i^{\text{dl}}(t))^2 \end{aligned} \quad (38)$$

Case II: when $Q_i(t+1) \geq 0$ and $Q_i(t) < 0$, we can achieve $\varphi C_{i,f_i}^{\text{th}}(t) - u_i^{\text{dl}}(t) > Q_i(t+1) \geq 0$, $[Q_i(t)]^+ = 0$ and

$$\begin{aligned} \frac{1}{2}([Q_i(t+1)]^+)^2 &< \frac{1}{2}(\varphi C_{i,f_i}^{\text{th}}(t) - u_i^{\text{dl}}(t))^2 \\ &= \frac{1}{2}([Q_i(t)]^+)^2 + [Q_i(t)]^+(\varphi C_{i,f_i}^{\text{th}}(t) - u_i^{\text{dl}}(t)) \\ &+ \frac{1}{2}(\varphi C_{i,f_i}^{\text{th}}(t) - u_i^{\text{dl}}(t))^2 \end{aligned} \quad (39)$$

Case III: when $Q_i(t+1) < 0$, we can obtain

$$\begin{aligned} \frac{1}{2}([Q_i(t+1)]^+)^2 &= 0 \\ &\leq \frac{1}{2}([Q_i(t)]^+ + (\varphi C_{i,f_i}^{\text{th}}(t) - u_i^{\text{dl}}(t)))^2 \\ &= \frac{1}{2}([Q_i(t)]^+)^2 + [Q_i(t)]^+(\varphi C_{i,f_i}^{\text{th}}(t) - u_i^{\text{dl}}(t)) \\ &+ \frac{1}{2}(\varphi C_{i,f_i}^{\text{th}}(t) - u_i^{\text{dl}}(t))^2 \end{aligned} \quad (40)$$

Therefore, we can have

$$\begin{aligned} \frac{1}{2}([Q_i(t+1)]^+)^2 &\leq \frac{1}{2}([Q_i(t)]^+)^2 \\ &+ [Q_i(t)]^+(\varphi C_{i,f_i}^{\text{th}}(t) - u_i^{\text{dl}}(t)) + \\ &\frac{1}{2}(\varphi C_{i,f_i}^{\text{th}}(t) - u_i^{\text{dl}}(t))^2 \end{aligned} \quad (41)$$

Similarly, according to (20), (21), and the non-negative operation, we have

$$\begin{aligned} \frac{1}{2}([Z_i(t+1)]^+)^2 &= \frac{1}{2}([Z_i(t)]^+)^2 + \\ &[Z_i(t)]^+(\gamma_i(t) - u_i^{\text{dl}}(t)) + \frac{1}{2}(\gamma_i(t) - u_i^{\text{dl}}(t))^2 \end{aligned} \quad (42)$$

and

$$\begin{aligned} \frac{1}{2}([H_j(t+1)]^+)^2 &\leq \frac{1}{2}([H_j(t)]^+)^2 \\ &+ [H_j(t)]^+(p_j(t) - \tilde{p}_j + p_j^c) + \frac{1}{2}(p_j(t) - \tilde{p}_j + p_j^c)^2 \end{aligned} \quad (43)$$

With inequalities (41)-(43), we can obtain a new inequality by utilizing the definition of Lyapunov drift. Next, we can achieve (24) by adding $-V \left(g(t) - \sum_{j=1}^N p_j(t) \right)$ to both sides of the new inequality. This completes the proof.

C. Proof of Proposition 2

For any given UAV transmit power $\mathcal{P}(t)$, UAV trajectories $\mathcal{X}(t-1)$ at time slot $t-1$, and the content delivery decision set $\mathcal{S}(t)$, we can optimize the variables $\mathcal{X}(t)$ in (27) via mitigating the following problem

$$\text{Maximize}_{\mathcal{X}(t)} \sum_i \{[Q_i(t)]^+ + [Z_i(t)]^+\} u_i^{\text{dl}}(t) \quad (44a)$$

$$\text{s.t. : } (5), (6), (9). \quad (44b)$$

To simplify (44a), we introduce slack variables $\{\eta_i\}$, with which (44) can be reformulated as

$$\text{Maximize}_{\mathcal{X}(t), \{\eta_i(t)\}} \sum_i \{[Q_i(t)]^+ + [Z_i(t)]^+\} \eta_i(t) \quad (45a)$$

$$\text{s.t. : } u_i^{\text{dl}}(t) \geq \eta_i(t), \forall i, t \quad (45b)$$

$$(5), (6), (9). \quad (45c)$$

Denote by η_i^* the optimal solution to (45). If η_i^* satisfies (45b) with strict inequality, we can then decrease $u_i^{\text{dl}}(t)$ to make (45b) active without changing the value of (45a). Therefore, (45) is equivalent to (44).

As $h_{ij}(t)$ can be rewritten as $h_{ij}(t) = \frac{\theta_{ij}}{g^2 + \|\mathbf{x}_j(t) - \mathbf{x}_i^u(t)\|^2}$, where $\theta_{ij} = \frac{G_L \phi_{SS}^2}{16\pi^2}$, the achievable data rate of user i can be expressed as $u_i^{\text{dl}}(t) = \sum_j s_{ij}(t) R_{ij}(t)$ with $R_{ij}(t) = \hat{R}_{ij}(t) - \log_2(\sigma^2 W + \sum_{k \in \mathcal{J} \setminus \{j\}} \frac{p_k(t) \theta_{ij}}{g^2 + \|\mathbf{x}_k(t) - \mathbf{x}_i^u(t)\|^2})$, and $\hat{R}_{ij}(t) = \log_2(\sigma^2 W + \sum_{k \in \mathcal{J}} \frac{p_k(t) \theta_{ij}}{g^2 + \|\mathbf{x}_k(t) - \mathbf{x}_i^u(t)\|^2})$.

(45) is not convex due to the non-convex constraint (6), and (45b). Therefore, we may not find efficient methods to obtain the optimal solution to (45). Although (45b) is not concave with w.r.t. $\mathbf{x}_j(t)$, we can observe that $\hat{R}_{ij}(t)$ is convex w.r.t. $\|\mathbf{x}_k(t) - \mathbf{x}_i^u(t)\|^2$. Accordingly, a slack variable $B_{ik}(t) = \|\mathbf{x}_k(t) - \mathbf{x}_i^u(t)\|^2 \forall i, k \neq j$ is involved to transform (45) into the following new problem

$$\text{Maximize}_{\mathcal{X}(t), \{\eta_i(t)\}, \{B_{ik}(t)\}} \sum_i \{[Q_i(t)]^+ + [Z_i(t)]^+\} \eta_i(t) \quad (46a)$$

$$\text{s.t. : } \sum_j s_{ij}(t) (\hat{R}_{ij}(t) + \tilde{R}_{ij}(t)) \geq \eta_i(t), \forall i, t \quad (46b)$$

$$B_{ik}(t) \leq \|\mathbf{x}_k(t) - \mathbf{x}_i^u(t)\|^2, \forall i, k \neq j, t \quad (46c)$$

$$(5), (6), (9). \quad (46d)$$

where $\tilde{R}_{ij}(t) = -\log_2(\sigma^2 W + \sum_{k \in \mathcal{J} \setminus \{j\}} \frac{p_k(t) \theta_{ij}}{g^2 + B_{ik}(t)})$.

Similar to (45), although a slack variable $B_{ik}(t)$ is introduced, (46) is equivalent to (45). Unfortunately, (46) is still non-convex as (6), (46b), and (46c) are non-convex.

To handle the non-convexity of (46), an SCA technique is explored. It can be observed that $\hat{R}_{ij}(t)$, $\forall i, j$ is convex w.r.t. $\|\mathbf{x}_k(t) - \mathbf{x}_i^u(t)\|^2$ and will be globally lower-bounded by its first-order Taylor expansion at any local point [36]. Therefore, for a given local point at the $(r+1)$ -th iteration ($r \geq 0$), denoted by $\mathbf{x}_k^{(r)}(t)$, $\hat{R}_{ij}(t)$ is lower-bounded by

$$\begin{aligned} \hat{R}_{ij}(t) &\geq \log_2 \left(\sigma^2 W + \sum_{k \in \mathcal{J}} \frac{p_k(t)\theta_{ij}}{g^2 + \|\mathbf{x}_k^{(r)}(t) - \mathbf{x}_i^u(t)\|^2} \right) \\ &- \sum_{k \in \mathcal{J}} \frac{\frac{p_k(t)\theta_{ij}}{(g^2 + \|\mathbf{x}_k^{(r)}(t) - \mathbf{x}_i^u(t)\|^2)^2 (\|\mathbf{x}_k(t) - \mathbf{x}_i^u(t)\|^2 - \|\mathbf{x}_k^{(r)}(t) - \mathbf{x}_i^u(t)\|^2)}{\left(\sigma^2 W + \sum_{k \in \mathcal{J}} \frac{p_k(t)\theta_{ij}}{g^2 + \|\mathbf{x}_k^{(r)}(t) - \mathbf{x}_i^u(t)\|^2} \right) \ln 2} \\ &= D_i^{(r)}(t) - \sum_{k \in \mathcal{J}} E_{ik}^{(r)}(t) (\|\mathbf{x}_k(t) - \mathbf{x}_i^u(t)\|^2 - \|\mathbf{x}_k^{(r)}(t) - \mathbf{x}_i^u(t)\|^2) \end{aligned} \quad (47)$$

where $D_i^{(r)}(t) = \log_2 \left(\sigma^2 W + \sum_{k \in \mathcal{J}} \frac{p_k(t)\theta_{ij}}{g^2 + \|\mathbf{x}_k^{(r)}(t) - \mathbf{x}_i^u(t)\|^2} \right)$ and $E_{ik}^{(r)}(t) = \frac{p_k(t)\theta_{ij}}{(g^2 + \|\mathbf{x}_k^{(r)}(t) - \mathbf{x}_i^u(t)\|^2)^2 2^{D_i^{(r)}(t)} \ln 2}$.

Besides, for a given location point $(\mathbf{x}_j^{(r)}(t), \mathbf{x}_k^{(r)}(t))$, we can obtain the lower bound of $\|\mathbf{x}_j(t) - \mathbf{x}_k(t)\|^2$ via the first order Taylor expansion as below

$$\begin{aligned} \|\mathbf{x}_j(t) - \mathbf{x}_k(t)\|^2 &\geq -\|\mathbf{x}_j^{(r)}(t) - \mathbf{x}_k^{(r)}(t)\|^2 + \\ &2(\mathbf{x}_j^{(r)}(t) - \mathbf{x}_k^{(r)}(t))^T (\mathbf{x}_j(t) - \mathbf{x}_k(t)). \end{aligned} \quad (48)$$

Similarly, for a given location point $\mathbf{x}_k^r(t)$, $\|\mathbf{x}_k(t) - \mathbf{x}_i^u(t)\|^2$ is lower-bounded by

$$\begin{aligned} \|\mathbf{x}_k(t) - \mathbf{x}_i^u(t)\|^2 &\geq \|\mathbf{x}_k^{(r)}(t) - \mathbf{x}_i^u(t)\|^2 + \\ &2(\mathbf{x}_k^{(r)}(t) - \mathbf{x}_i^u(t))^T (\mathbf{x}_k(t) - \mathbf{x}_i^u(t)). \end{aligned} \quad (49)$$

For any local point $\mathcal{X}^{(r)}(t) = \{\mathbf{x}_k^{(r)}(t)\}$, by referring to (47)-(49), (46) can be approximated as (32). This completes the proof.

D. Proof of Proposition 3

For any given content delivery decision set $\mathcal{S}(t)$ as well as UAV trajectories $\mathcal{X}(t)$, the UAV transmit power of (16) can be optimized via mitigating the following problem

$$\begin{aligned} \text{Maximize}_{\mathcal{P}(t), \{\eta_i(t)\}} & -V\rho \sum_j p_j(t) - \sum_j [H_j(t)]^+ p_j(t) + \\ & \sum_i \{[Q_i(t)]^+ + [Z_i(t)]^+\} \eta_i(t) \end{aligned} \quad (50a)$$

$$\begin{aligned} \text{s.t. : } & \sum_j s_{ij}(t) \log_2 \left(1 + \frac{p_j(t)h_{ij}(t)}{\sigma^2 W + \sum_{k \in \mathcal{J} \setminus \{j\}} p_k(t)h_{ik}(t)} \right) \\ & \geq \eta_i(t), \quad i, t \end{aligned} \quad (50b)$$

$$\eta_i(t) \geq s_{ij}(t) C_{i, f_i}^{\text{th}}(t), \quad i, j, t \quad (50c)$$

$$(16d), (16g) \quad (50d)$$

where (50c) is enforced due to the data rate requirement of enabling a user's desired QoE state.

Owing to the non-convex constraint (50b), (50) is non-convex; as a result, it is challenging to achieve its optimal

solution. However, we observe that (50b) is a difference of two concave functions w.r.t. $p_k(t)$. Accordingly, we adopt the SCA technique again to approximate (50b). Specifically, $\widetilde{R}_{ij}(t)$ can be rewritten as $R_{ij}(t) = \hat{R}_{ij}(t) - \widetilde{R}_{ij}(t)$, where $\hat{R}_{ij}(t) = \log_2 \left(\sigma^2 W + \sum_{k \in \mathcal{J} \setminus \{j\}} p_k(t)h_{ik}(t) \right)$. For any local point $\mathcal{P}^{(r)}(t) = \{p_j^r(t)\}$, via the first order Taylor expansion $\widetilde{R}_{ij}(t)$ is upper-bounded by

$$\begin{aligned} \widetilde{R}_{ij}(t) &\leq \log_2 \left(\sigma^2 W + \sum_{k \in \mathcal{J} \setminus \{j\}} p_k^{(r)}(t)h_{ik}(t) \right) \\ &+ \sum_{k \in \mathcal{J} \setminus \{j\}} \frac{h_{ik}(t) \ln^{-1} 2}{\sigma^2 W + \sum_{k \in \mathcal{J} \setminus \{j\}} p_k^{(r)}(t)h_{ik}(t)} (p_k(t) - p_k^{(r)}(t)) \\ &= F_{ij}^{(r)}(t) + \sum_{k \in \mathcal{J} \setminus \{j\}} G_{ik}^{(r)}(t) (p_k(t) - p_k^{(r)}(t)) \end{aligned} \quad (51)$$

where $F_{ij}^{(r)}(t) = \log_2 \left(\sigma^2 W + \sum_{k \in \mathcal{J} \setminus \{j\}} p_k^{(r)}(t)h_{ik}(t) \right)$ and $G_{ik}^{(r)}(t) = \frac{h_{ik}(t)}{2^{F_{ij}^{(r)}(t)} \ln 2}$.

We can thus write the lower bound of $R_{ij}(t)$ as $R_{ij}(t) \geq \hat{R}_{ij}(t) - F_{ij}^{(r)}(t) - \sum_{k \in \mathcal{J} \setminus \{j\}} G_{ik}^{(r)}(t)(p_k(t) - p_k^{(r)}(t))$.

In summary, for any local point $\mathcal{P}^{(r)}(t)$, (50) can be approximated as (33). This completes the proof.

E. Proof of Lemma 2

Given a local point $(\mathcal{X}^{(r)}(t), \mathcal{P}^{(r)}(t))$, the obtained value of (31a) at the $(r+1)$ -th iteration, denoted by $\Gamma(\mathcal{S}^{(r+1)}(t), \mathcal{X}^{(r)}(t), \mathcal{P}^{(r)}(t))$, is no greater than $\Gamma(\mathcal{S}^{(r+1)}(t), \mathcal{X}^{(r)}(t), \mathcal{P}^{(r)}(t))$ via optimizing (31). Given a point $(\mathcal{S}^{(r+1)}(t), \mathcal{P}^{(r)}(t))$, we have $\Gamma(\mathcal{S}^{(r+1)}(t), \mathcal{X}^{(r)}(t), \mathcal{P}^{(r)}(t)) \geq \Gamma(\mathcal{S}^{(r+1)}(t), \mathcal{X}^{(r+1)}(t), \mathcal{P}^{(r)}(t))$ due to the minimization of the upper-bounded problem of (45). Likewise, the inequality $\Gamma(\mathcal{S}^{(r+1)}(t), \mathcal{X}^{(r+1)}(t), \mathcal{P}^{(r+1)}(t)) \geq \Gamma(\mathcal{S}^{(r+1)}(t), \mathcal{X}^{(r+1)}(t), \mathcal{P}^{(r)}(t))$ can be obtained at $(\mathcal{S}^{(r+1)}(t), \mathcal{X}^{(r+1)}(t))$. Besides, $\Gamma(\mathcal{S}^{(r)}(t), \mathcal{X}^{(r)}(t), \mathcal{P}^{(r)}(t))$ is bounded at each iteration. Therefore, Algorithm 1 is convergent.

Lemma 1 points out that $\Delta(t) - V(g(t) - \rho \sum_j p_j^{\text{tot}}(t))$ is upper-bounded at each time slot t . The time average of $L(t)$ then tends to be zero when $t \rightarrow \infty$. Therefore, Algorithm 2 can make all virtual queues mean-rate stable. This completes the proof.

F. Proof of Lemma 3

According to the evolution model in (34), $N_a^1 = 0$. Therefore, we focus on deriving the close-form expression of N_a^q with $q > 1$. During the 2-nd time interval, $n = 0$ indicates that there are no new arrivals or n_c new arrivals during the 1-st time interval; $n > 0$ means that the number of new arrivals in the 1-st time interval is $n + n_c$. Therefore, the probability mass function (PMF) of the accumulated packets, denoted as $f_{N_a^2}(n)$, can be expressed as

$$f_{N_a^2}(n) = \begin{cases} e^{-\vartheta_w^1} + \vartheta_w^1 e^{-\vartheta_w^1}, & n = 0 \\ \frac{(\vartheta_w^1)^{n+n_c} e^{-\vartheta_w^1}}{(n+n_c)!}, & n > 0 \end{cases} \quad (52)$$

Similarly, in the 3-rd time interval, three cases will result in $n = 0$: Case I, both the accumulate number of packets and the

number of new arrivals in the 2-nd time interval are zero; Case II, the accumulated number of packets is n_c and the number of new arrivals is zero in the 2-nd time interval; Case III, the accumulated number of packets is zero while the number of new arrivals is n_c in the 2-nd time interval. $n > 0$ indicates that the sum of the accumulated number of packets and the number of new arrivals in the 2-nd time interval is $n + n_c$. Therefore, we can obtain the PMF of the accumulate number of packets, denoted by $f_{N_a^3}(n)$, in the 3-rd time interval as follows

$$f_{N_a^3}(n) = \begin{cases} e^{-\vartheta_w^2} f_{N_a^2}(0) + \vartheta_w^2 e^{-\vartheta_w^2} f_{N_a^2}(0) + & n = 0 \\ e^{-\vartheta_w^2} f_{N_a^2}(n_c), & \\ \sum_{z=0}^{n+n_c} \frac{(\vartheta_w^2)^z}{z!} e^{-\vartheta_w^2} f_{N_a^2}(n + n_c - z), & n > 0 \end{cases} \quad (53)$$

Likewise, in the q -th time interval, we can obtain the PMF of the accumulated number of packets, denoted by $f_{N_a^q}(n)$, as follows

$$f_{N_a^q}(n) = \begin{cases} e^{-\vartheta_w^{q-1}} f_{N_a^{q-1}}(0) + \vartheta_w^{q-1} e^{-\vartheta_w^{q-1}} \times & n = 0 \\ f_{N_a^{q-1}}(0) + e^{-\vartheta_w^{q-1}} f_{N_a^{q-1}}(n_c), & \\ \sum_{z=0}^{n+n_c} \frac{(\vartheta_w^{q-1})^z}{z!} e^{-\vartheta_w^{q-1}} f_{N_a^{q-1}}(n + n_c - z), & n > 0 \end{cases} \quad (54)$$

In (54), $f_{N_a^q}(n)$ correlates with $f_{N_a^{q-1}}(n + n_c - z)$ in a sophisticated recursive way, which significantly hinders the theoretical derivation of the closed-form expression of $f_{N_a^q}(n)$. Moreover, the complexity of the theoretical derivation exponentially increases with q . To tackle this problem, we propose to derive an approximated expression of $f_{N_a^q}(n)$. As new packets arrive in a Poisson process, the packet departure can be considered as an approximated packet thinning of the arrived packets [37], [38]. After this packet thinning in a specific time interval, the number of accumulated packets in time q ($q > 1$) can be approximated as a Poisson distribution [38]. Then, denote by ϑ_a^q the average number of accumulated packets in time q . In the 2-nd time interval, we can calculate ϑ_a^2 as

$$\begin{aligned} \vartheta_a^2 &\stackrel{(a)}{=} \sum_{n=1}^{\infty} (n - n_c) \frac{(\vartheta_w^1)^n e^{-\vartheta_w^1}}{n!} \\ &= \sum_{n=0}^{\infty} n \frac{(\vartheta_w^1)^n e^{-\vartheta_w^1}}{n!} - n_c \left(\sum_{n=0}^{\infty} \frac{(\vartheta_w^1)^n e^{-\vartheta_w^1}}{n!} - e^{-\vartheta_w^1} \right) \\ &\stackrel{(b)}{=} \left[\vartheta_w^1 - n_c \left(1 - e^{-\vartheta_w^1} \right) \right]^+ \end{aligned} \quad (55)$$

where (a) holds because $\Pr\{N_a^2 = n - n_c\} = \Pr\{N_w^1 = n\}$ if $n \neq 0$ with $\Pr\{x\}$ denoting the probability of event x , and (b) holds because ϑ_a^2 is non-negative at each time slot t .

In the 3-rd time interval, the intensity of accumulated data packets in the preprocessing queue can be derived as the following

$$\begin{aligned} \vartheta_a^3 &= \sum_{n=1}^{\infty} (n - n_c) \sum_{z=0}^n \frac{(\vartheta_w^2)^z e^{-\vartheta_w^2}}{z!} \frac{(\vartheta_a^2)^{n-z} e^{-\vartheta_a^2}}{(n-z)!} \\ &= \sum_{n=1}^{\infty} n \sum_{z=0}^n \frac{(\vartheta_w^2)^z e^{-\vartheta_w^2}}{z!} \frac{(\vartheta_a^2)^{n-z} e^{-\vartheta_a^2}}{(n-z)!} - \\ n_c &\left(\sum_{n=0}^{\infty} \sum_{z=0}^n \frac{(\vartheta_w^2)^z e^{-\vartheta_w^2}}{z!} \frac{(\vartheta_a^2)^{n-z} e^{-\vartheta_a^2}}{(n-z)!} - e^{-\vartheta_w^2 - \vartheta_a^2} \right) \\ &= \left[\vartheta_w^2 + \vartheta_a^2 - n_c \left(1 - e^{-\vartheta_w^2 - \vartheta_a^2} \right) \right]^+ \end{aligned} \quad (56)$$

When $q > 3$, since the accumulated packet evolution model of the preprocessing queue is similar to that at $q = 3$, we can extend the conclusion obtained at $q = 3$ to that at $q > 3$. Therefore, we can obtain the closed-form expression of ϑ_a^q at $q > 3$ with

$$\vartheta_a^q = \left[\vartheta_w^{q-1} + \vartheta_a^{q-1} - n_c \left(1 - e^{-\vartheta_w^{q-1} - \vartheta_a^{q-1}} \right) \right]^+ \quad (57)$$

Besides, at time q , for packet m , it has to wait until the completion of the preprocessing of accumulated packets in the preprocessing queue according to the FCFS principle. The preprocessing time of each packet is $Y_{i,m}^S$ due to the same packet size and preprocessing operation. Thus, the average packet queueing delay of packet m is $\vartheta_a^q Y_{i,m}^S$. This completes the proof.

G. Proof of Proposition 4

For packet m , it will be delivered to its receiving user i if and only if a) m has been processed by the BS; b) $\sum_j s_{ij}(t) = 1$ at time slot t . As there are N users and J UAVs and the goal of the communication problem is to provide fair content delivery for all users, the probability that any user can connect to a UAV is J/N at each time slot. The delivery of a content file including L/l packets from the BS or a UAV to its corresponding user should be completed in a time slot of duration Δ_t . Further, one packet will be sent to user i at a time, and L/l packets will be sequentially delivered in duration Δ_t . Then, we have $\mathbb{E}[Y_{i,1}^A] = \frac{Nl\Delta_t}{JL}$, and the expected edge arrival duration of the last packet of the content file is $\frac{N\Delta_t}{J}$. Thus, for any packet m in the content file transmitted to user i , the expected edge arrival duration of packet m is $\frac{Nl\Delta_t}{2JL} + \frac{N\Delta_t}{2J}$. This completes the proof.

H. Proof of Lemma 4

By referring to (15), we can write the expectation of PAoI of packet m sent to i as follows

$$\begin{aligned} \Delta_{i,m}(\hat{q}; q) &= \mathbb{E}[X_{i,m}] + \mathbb{E}[Y_{i,m}] \\ &= \mathbb{E}[X_{i,m}] + \mathbb{E}[Y_{i,m}^Q] + \mathbb{E}[Y_{i,m}^S] + \mathbb{E}[Y_{i,m}^A] \end{aligned} \quad (58)$$

Next, we discuss the value of $\Delta_{i,m}(\hat{q}; q)$ from the following two cases:

Case I: $q = 1$ and $m = 1$. The value of $\Pr\{M(q) = 0\}$ will become smaller as q increases, where $M(q)$ denotes the number of newly arrived packets before time q . For example, according to (55), the average number of accumulated packets in the preprocessing queue is $[\vartheta_w^1 - n_c(1 - e^{-\vartheta_w^1})]^+$ when $q = 2$. Besides, the content server will generate packets required by a user after receiving its content request. It indicates that the probability that the content server generates packets destined to i during each time interval is equal to $\Pr_i, \forall i$. Then, the expected number of new packets is $\vartheta_w^1 + n_c e^{-\vartheta_w^1}$, and the number of packets sent to user i is $M_i(q) = (\vartheta_w^1 + n_c e^{-\vartheta_w^1}) \Pr_i$, where $M_i(q)$ is the expected number of packets destined to user i . We can envision that the expected number of generated packets sent to user i will be greater than $(\vartheta_w^1 + n_c e^{-\vartheta_w^1}) \Pr_i$ when $q > 2$. Recall that the content server generates packets according to a Poisson process with

rate ϑ_w^q at time q and sends them to the BS. The generated packets can be considered to be belonging to N different data streams for N terrestrial users, respectively. Each data stream i is chosen independently at time q with probability Pr_i . This setup is equivalent to having N independent Poisson sources with rates $\lambda_i^q = \vartheta_w^q \text{Pr}_i$, $\forall i$, and $\vartheta_w^q = \lambda_1^q + \dots + \lambda_N^q$ (see [39]). Thus, we have $\text{Pr}\{N_i(q) = m\} = \frac{(\vartheta_w^q \text{Pr}_i)^m}{m!} e^{-\vartheta_w^q \text{Pr}_i}$ and $\text{Pr}\{N_i(1) = 0\} = 1/e^{\vartheta_w^1 \text{Pr}_i}$, which will be a small value. It indicates that the event that the content server does not generate the first packet for user i in the 1-st time interval is a small probability event. We therefore consider the case of $q = 1$ and $m = 1$. On the other hand, according to (34), the accumulated packets in the preprocessing queue is zero when $q = 1$. Therefore, the expected time for the first packet destined to user i includes the preprocessing time and the expected edge arrival duration, i.e., we can obtain

$$\begin{aligned} \mathbb{E}[\Delta_{i,1}(\hat{1}; 1)] &= \mathbb{E}[Y_{i,1}^S] + \mathbb{E}[Y_{i,m}^A] \\ &= \frac{1}{n_c} + \frac{(l+L)N\Delta_t}{2JL} \end{aligned} \quad (59)$$

Case II: $q > 1$ and $m > 1$. As the inter-arrival time of packets destined to user i from the content server follows an exponential distribution with intensity λ_i^q , we have $\mathbb{E}[X_{i,m}] = 1/\lambda_i^q$. Besides, since each packet has the same size, the expected preprocessing time for each packet will be the same, i.e., $\mathbb{E}[Y_{i,m}^S] = 1/n_c$. From Lemma 3, we know that the average packet queuing delay of packet m is $\vartheta_a^q Y_{i,m}^S$. Thus, we have $\mathbb{E}[Y_{i,m}^Q] = \vartheta_a^q/n_c$. Proposition 4 also shows that $\mathbb{E}[Y_{i,m}^A] = \frac{(l+L)N\Delta_t}{2JL} \forall i, m$. Therefore, (37) is obtained. This completes the proof.

REFERENCES

- [1] P. Yang, X. Xi, T. Q. S. Quek, J. Chen, X. Cao, and D. Wu, "Repeatedly energy-efficient and fair service coverage: Uav slicing," in *GLOBECOM 2020-2020 IEEE Global Communications Conference*. IEEE, 2020, pp. 1–6.
- [2] Cisco, "Cisco visual networking index: global mobile data traffic forecast update, 2017–2022," <https://davidellis.ca/wp-content/uploads/2019/12/cisco-vni-mobile-data-traffic-feb-2019.pdf>, 2019.
- [3] J. Ji, K. Zhu, D. Niyato, and R. Wang, "Joint cache placement, flight trajectory and transmission power optimization for multi-UAV assisted wireless networks," *IEEE Transactions on Wireless Communications*, vol. 19, no. 8, pp. 5389–5403, 2020.
- [4] X. Cao, P. Yang, M. Alzenad, X. Xi, D. Wu, and H. Yanikomeroglu, "Airborne communication networks: A survey," *IEEE Journal on Selected Areas in Communications*, vol. 36, no. 9, pp. 1907–1926, 2018.
- [5] H. Wu, F. Lyu, C. Zhou, J. Chen, L. Wang, and X. Shen, "Optimal UAV caching and trajectory in aerial-assisted vehicular networks: A learning-based approach," *IEEE Journal on Selected Areas in Communications*, vol. 38, no. 12, pp. 2783–2797, 2020.
- [6] M. Aloqaily, O. Bouachir, A. Boukerche, and I. Al Ridhawi, "Design guidelines for blockchain-assisted 5G-UAV networks," *IEEE Network*, vol. 35, no. 1, pp. 64–71, 2021.
- [7] J. Urama, R. Wiren, O. Galinina, J. Kauppi, K. Hiltunen, J. Erkkila, F. Chernogorov, P. Etelaaho, M. Heikkila, J. Torsner *et al.*, "UAV-aided interference assessment for private 5G NR deployments: Challenges and solutions," *IEEE Communications Magazine*, vol. 58, no. 8, pp. 89–95, 2020.
- [8] R. Amorim, I. Z. Kovács, J. Wigard, T. B. Sorensen, and P. Mogensen, "Forecasting spectrum demand for UAVs served by dedicated allocation in cellular networks," in *2019 IEEE Wireless Communications and Networking Conference Workshop (WCNCW)*. IEEE, 2019, pp. 1–6.
- [9] R. de Silva and S. Rajasinghege, "Optimal desired trajectories of UAVs in private UAV networks," in *2018 International Conference on Advanced Technologies for Communications (ATC)*. IEEE, 2018, pp. 310–314.
- [10] B. Jiang, J. Yang, H. Xu, H. Song, and G. Zheng, "Multimedia data throughput maximization in Internet-of-Things system based on optimization of cache-enabled UAV," *IEEE Internet of Things Journal*, vol. 6, no. 2, pp. 3525–3532, 2018.
- [11] L. Wang, H. Wu, Z. Han, P. Zhang, and H. V. Poor, "Multi-hop cooperative caching in social IoT using matching theory," *IEEE Transactions on Wireless Communications*, vol. 17, no. 4, pp. 2127–2145, 2017.
- [12] J. Ji, K. Zhu, D. Niyato, and R. Wang, "Joint trajectory design and resource allocation for secure transmission in cache-enabled UAV-relaying networks with D2D communications," *IEEE Internet of Things Journal*, 2020, in Press. DOI: 10.1109/JIOT.2020.3013647.
- [13] S. Chai and V. K. Lau, "Online trajectory and radio resource optimization of cache-enabled UAV wireless networks with content and energy recharging," *IEEE Transactions on Signal Processing*, vol. 68, pp. 1286–1299, 2020.
- [14] E. Kalantari, H. Yanikomeroglu, and A. Yongacoglu, "Wireless networks with cache-enabled and backhaul-limited aerial base stations," *IEEE Transactions on Wireless Communications*, vol. 19, no. 11, pp. 7363–7376, 2020.
- [15] H. Hu, K. Xiong, G. Qu, Q. Ni, P. Fan, and K. B. Letaief, "AoI-minimal trajectory planning and data collection in UAV-assisted wireless powered IoT networks," *IEEE Internet of Things Journal*, vol. 8, no. 2, pp. 1211–1223, 2021.
- [16] M. Samir, C. Assi, S. Sharafeddine, and A. Ghreyeb, "Online altitude control and scheduling policy for minimizing AoI in UAV-assisted IoT wireless networks," *IEEE Transactions on Mobile Computing*, 2020, in Press. DOI: 10.1109/TMC.2020.3042925.
- [17] S. Kaul, R. Yates, and M. Gruteser, "Real-time status: How often should one update?" in *2012 Proceedings IEEE INFOCOM*. IEEE, 2012, pp. 2731–2735.
- [18] S. Zhang, H. Zhang, Z. Han, H. V. Poor, and L. Song, "Age of information in a cellular Internet of UAVs: Sensing and communication trade-off design," *IEEE Transactions on Wireless Communications*, vol. 19, no. 10, pp. 6578–6592, 2020.
- [19] P. Rost, C. Mannweiler, D. S. Michalopoulos, C. Sartori, V. Sciancalepore, N. Sastry, O. Holland, S. Tayade, B. Han, D. Bega *et al.*, "Network slicing to enable scalability and flexibility in 5G mobile networks," *IEEE Communications magazine*, vol. 55, no. 5, pp. 72–79, 2017.
- [20] P. Schneider, C. Mannweiler, and S. Kerboeuf, "Providing strong 5G mobile network slice isolation for highly sensitive third-party services," in *2018 IEEE Wireless Communications and Networking Conference (WCNC)*. IEEE, 2018, pp. 1–6.
- [21] B. Aboba, L. Blunk, J. Vollbrecht, J. Carlson, H. Levkowitz *et al.*, "Extensible authentication protocol (EAP)," Tech. Rep. RFC 3748, June, 2004.
- [22] 3GPP, "Security architecture and procedures for 5G system," The 3rd Generation Partnership Project, Tech. Rep. 33.501, Dec. 2020.
- [23] ETSI, "Network functions virtualisation (NFV): Architectural framework," https://www.etsi.org/deliver/etsi_gs/nfv/001_099/002/01.01.01_60/gs_nfv002v010101p.pdf, 2013.
- [24] T. Taleb, K. Samdanis, B. Mada, H. Flinck, S. Dutta, and D. Sabella, "On multi-access edge computing: A survey of the emerging 5G network edge cloud architecture and orchestration," *IEEE Communications Surveys & Tutorials*, vol. 19, no. 3, pp. 1657–1681, 2017.
- [25] M. Ma and V. W. Wong, "Age of information driven cache content update scheduling for dynamic contents in heterogeneous networks," *IEEE Transactions on Wireless Communications*, vol. 19, no. 2, pp. 8427–8441, 2020.
- [26] M. Chen, M. Mozaffari, W. Saad, C. Yin, M. Debbah, and C. S. Hong, "Caching in the sky: Proactive deployment of cache-enabled unmanned aerial vehicles for optimized quality-of-experience," *IEEE Journal on Selected Areas in Communications*, vol. 35, no. 5, pp. 1046–1061, 2017.
- [27] A. Al-Hourani, S. Kandeepan, and S. Lardner, "Optimal LAP altitude for maximum coverage," *IEEE Wireless Communications Letters*, vol. 3, no. 6, pp. 569–572, 2014.
- [28] K. Mitra, A. Zaslavsky, and C. Åhlund, "Context-aware QoE modelling, measurement, and prediction in mobile computing systems," *IEEE Transactions on Mobile Computing*, vol. 14, no. 5, pp. 920–936, 2013.
- [29] X. Xi, X. Cao, P. Yang, J. Chen, T. Q. Quek, and D. Wu, "Network resource allocation for eMBB payload and URLLC control information communication multiplexing in a multi-UAV relay network," *IEEE Transactions on Communications*, 2020, in Press. DOI: 10.1109/TCOMM.2020.3042970.
- [30] C. Xu, H. H. Yang, X. Wang, and T. Q. Quek, "Optimizing information freshness in computing-enabled IoT networks," *IEEE Internet of Things Journal*, vol. 7, no. 2, pp. 971–985, 2019.

- [31] R. Talak, S. Karaman, and E. Modiano, "Optimizing information freshness in wireless networks under general interference constraints," *IEEE/ACM Transactions on Networking*, vol. 28, no. 1, pp. 15–28, 2019.
- [32] M. J. Neely, "A Lyapunov optimization approach to repeated stochastic games," in *2013 51st Annual Allerton Conference on Communication, Control, and Computing (Allerton)*. IEEE, 2013, pp. 1082–1089.
- [33] C. J. Watkins and P. Dayan, "Q-learning," *Machine learning*, vol. 8, no. 3-4, pp. 279–292, 1992.
- [34] T. P. Lillicrap, J. J. Hunt, A. Pritzel, N. Heess, T. Erez, Y. Tassa, D. Silver, and D. Wierstra, "Continuous control with deep reinforcement learning," *Computer Science*, vol. 8, no. 6, p. A187, 2015.
- [35] G. Scutari, F. Facchinei, and L. Lampariello, "Parallel and distributed methods for constrained nonconvex optimization-part I: Theory," *IEEE Transactions on Signal Processing*, vol. 65, no. 8, pp. 1929–1944, 2016.
- [36] B. Stephen and V. Lieven, *Convex Optimization*. Cambridge University Press, 2004.
- [37] N. Hohn and D. Veitch, "Inverting sampled traffic," *IEEE/ACM Transactions on Networking*, vol. 14, no. 1, pp. 68–80, 2006.
- [38] N. Jiang, Y. Deng, X. Kang, and A. Nallanathan, "Random access analysis for massive IoT networks under a new spatio-temporal model: A stochastic geometry approach," *IEEE Transactions on Communications*, vol. 66, no. 11, pp. 5788–5803, 2018.
- [39] S. M. Ross, J. J. Kelly, R. J. Sullivan, W. J. Perry, D. Mercer, R. M. Davis, T. D. Washburn, E. V. Sager, J. B. Boyce, and V. L. Bristow, *Stochastic processes*. Wiley New York, 1996, vol. 2.